the course of experimental autoimmune myocarditis in rats. *J Mol Cell Cardiol*. 1997;29:491–502.
4. Lauer B, Padberg K, Schultheiss HP, Strauer BE. Autoantibodies against human ventricular myosin in sera of patients with acute and chronic myocarditis. *J Am Coll Cardiol*. 1994;23:146–153.
5. Kodama M, Matsumoto Y, Fujiwara M, Masani F, Izumi T, Shibata A. A novel experimental model of giant cell myocarditis induced in rats by immunization with cardiac myosin fraction. *Clin Immunol Immunopathol*. 1990;57:250–262.
6. Nakamura T, Nawa K, Ichihara A. Partial purification and characterization of hepatocyte growth factor from serum of hepatectomized rats. *Biochem Biophys Res Commun*. 1984;122:1450–1459.
7. Nakamura T, Nishizawa T, Hagiya M, Seki T, Shimonishi M, Sugimura A, Tashiro K, Shimizu S. Molecular cloning and expression of human hepatocyte growth factor. *Nature*. 1989;342:440–443.
8. Birchmeier C, Gherardi E. Developmental roles of HGF/SF and its receptor, the c-Met tyrosine kinase. *Trends Cell Biol*. 1998;8:404–410.
9. Kosai K, Matsumoto K, Funakoshi H, Nakamura T. Hepatocyte growth factor prevents endotoxin-induced lethal hepatic failure in mice. *Hepatology*. 1999;30:151–159.
10. Bottaro DP, Rubin JS, Faletto DL, Chan AM, Kmiecik TE, Vande Woude GF, Aaronson SA. Identification of the hepatocyte growth factor receptor as the c-met proto-oncogene product. *Science*. 1991;251:802–804.
11. Yoshimura R, Watanabe Y, Kasai S, Wada S, Ohyama A, Hase T, Nakatani T, Chargui J, Touraine JL, Nakamura T. Hepatocyte growth factor (HGF) as a rapid diagnostic marker and its potential in the prevention of acute renal rejection. *Transpl Int*. 2002;15:156–162.
12. Kuroiwa T, Kakishita E, Hamano T, Kataoka Y, Seto Y, Iwata N, Kaneda Y, Matsumoto K, Nakamura T, Ueki T, Fujimoto J, Iwasaki T. Hepatocyte growth factor ameliorates acute graft-versus-host disease and promotes hematopoietic function. *J Clin Invest*. 2001;107:1365–1373.
13. Morishita R, Nakamura S, Hayashi S, Taniyama Y, Moriguchi A, Nagano T, Taiji M, Noguchi H, Takeshita S, Matsumoto K, Nakamura T, Higaki J, Ogihara T. Therapeutic angiogenesis induced by human recombinant hepatocyte growth factor in rabbit hind limb ischemia model as cytokine supplement therapy. *Hypertension*. 1999;33:1379–1384.
14. Nakamura T, Mizuno S, Matsumoto K, Sawa Y, Matsuda H. Myocardial protection from ischemia/reperfusion injury by endogenous and exogenous HGF. *J Clin Invest*. 2000;106:1511–1519.
15. Li Y, Takemura G, Kosai K, Yuge K, Nagano S, Esaki M, Goto K, Takahashi T, Hayakawa K, Koda M, Kawase Y, Maruyama R, Okada H, Minatoguchi S, Mizuguchi H, Fujiwara T, Fujiwara H. Postinfarction treatment with an adenoviral vector expressing hepatocyte growth factor relieves chronic left ventricular remodeling and dysfunction in mice. *Circulation*. 2003;107:2499–2506.
16. Yamaura K, Ito K, Tsukioka K, Wada Y, Makiuchi A, Sakaguchi M, Akashima T, Fujimori M, Sawa Y, Morishita R, Matsumoto K, Nakamura T, Suzuki J, Amano J, Isobe M. Suppression of acute and chronic rejection by hepatocyte growth factor in a murine model of cardiac transplantation: induction of tolerance and prevention of cardiac allograft vasculopathy. *Circulation*. 2004;110:1650–1657.
17. Yokoseki O, Suzuki J, Kitabayashi H, Watanabe N, Wada Y, Aoki M, Morishita R, Kaneda Y, Ogihara T, Futamatsu H, Kobayashi Y, Isobe M. cis Element decoy against nuclear factor-kappaB attenuates development of experimental autoimmune myocarditis in rats. *Circ Res*. 2001;89:899–906.
18. Futamatsu H, Suzuki J, Kosuge H, Yokoseki O, Kamada M, Ito H, Inobe M, Isobe M, Uede T. Attenuation of experimental autoimmune myocarditis by blocking activated T cells through inducible costimulatory molecule pathway. *Cardiovasc Res*. 2003;59:95–104.
19. Kosuge H, Suzuki J, Kakuta T, Haraguchi G, Koga N, Futamatsu H, Gotoh R, Inobe M, Isobe M, Uede T. Attenuation of graft arterial disease by manipulation of the LIGHT pathway. *Arterioscler Thromb Vasc Biol*. 2004;24:1409–1415.
20. Kaneda Y, Nakajima T, Nishikawa T, Yamamoto S, Ikegami H, Suzuki N, Nakamura H, Morishita R, Kotani H. Hemagglutinating virus of Japan (HVJ) envelope vector as a versatile gene delivery system. *Mol Ther*. 2002;6:219–226.
21. Seki T, Hagiya M, Shimonishi M, Nakamura T, Shimizu S. Organization of the human hepatocyte growth factor-encoding gene. *Gene*. 1991;102:213–219.
22. Maejima Y, Adachi S, Ito H, Nobori K, Tamamori-Adachi M, Isobe M. Nitric oxide inhibits ischemia/reperfusion-induced myocardial apoptosis by modulating cyclin A-associated kinase activity. *Cardiovasc Res*. 2003;59:308–320.
23. Parsa CJ, Matsumoto A, Kim J, Riel RU, Pascal LS, Walton GB, Thompson RB, Petrofski JA, Annex BH, Stamler JS, Koch WJ. A novel protective effect of erythropoietin in the infarcted heart. *J Clin Invest*. 2003;112:999–1007.
24. Hecht TT, Longo DL, Matis LA. The relationship between immune interferon production and proliferation in antigen-specific, MHC-restricted T cell lines and clones. *J Immunol*. 1983;131:1049–1055.
25. Kono S, Nagaike M, Matsumoto K, Nakamura T. Marked induction of hepatocyte growth factor mRNA in intact kidney and spleen in response to injury of distant organs. *Biochem Biophys Res Commun*. 1992;186:991–998.
26. Liu Y, Tolbert EM, Lin L, Thursby MA, Sun AM, Nakamura T, Dworkin LD. Up-regulation of hepatocyte growth factor receptor: an amplification and targeting mechanism for hepatocyte growth factor action in acute renal failure. *Kidney Int*. 1999;55:442–453.
27. Boccaccio C, Gaudino G, Gambarotta G, Galimi F, Comoglio PM. Hepatocyte growth factor (HGF) receptor expression is inducible and is part of the delayed-early response to HGF. *J Biol Chem*. 1994;269:12846–12851.
28. Okura Y, Takeda K, Honda S, Hanawa H, Watanabe H, Kodama M, Izumi T, Aizawa Y, Seki S, Abo T. Recombinant murine interleukin-12 facilitates induction of cardiac myosin-specific type 1 helper T cells in rats. *Circ Res*. 1998;82:1035–1042.
29. Ueki T, Kaneda Y, Tsutsui H, Nakanishi K, Sawa Y, Morishita R, Matsumoto K, Nakamura T, Takahashi H, Okamoto E, Fujimoto J. Hepatocyte growth factor gene therapy of liver cirrhosis in rats. *Nat Med*. 1999;5:226–230.
30. Hayashi S, Morishita R, Higaki J, Aoki M, Moriguchi A, Kida I, Yoshiki S, Matsumoto K, Nakamura T, Kaneda Y, Ogihara T. Autocrine-paracrine effects of overexpression of hepatocyte growth factor gene on growth of endothelial cells. *Biochem Biophys Res Commun*. 1996;220:539–545.
31. Liblau RS, Singer SM, McDevitt HO. Th1 and Th2 CD4+ T cells in the pathogenesis of organ-specific autoimmune diseases. *Immunol Today*. 1995;16:34–38.
32. Watanabe K, Nakazawa M, Fuse K, Hanawa H, Kodama M, Aizawa Y, Ohnuki T, Gejyo F, Maruyama H, Miyazaki J. Protection against autoimmune myocarditis by gene transfer of interleukin-10 by electroporation. *Circulation*. 2001;104:1098–1100.
33. Ueda H, Nakamura T, Matsumoto K, Sawa Y, Matsuda H. A potential cardioprotective role of hepatocyte growth factor in myocardial infarction in rats. *Cardiovasc Res*. 2001;51:41–50.
34. Duan HF, Wu CT, Wu DL, Lu Y, Liu HJ, Ha XQ, Zhang QW, Wang H, Jia XX, Wang LS. Treatment of myocardial ischemia with bone marrow-derived mesenchymal stem cells overexpressing hepatocyte growth factor. *Mol Ther*. 2003;8:467–474.
35. Miyagawa S, Sawa Y, Taketani S, Kawaguchi N, Nakamura T, Matsuura N, Matsuda H. Myocardial regeneration therapy for heart failure: hepatocyte growth factor enhances the effect of cellular cardiomyoplasty. *Circulation*. 2002;105:2556–2561.

nature medicine

G-CSF prevents cardiac remodeling after myocardial infarction by activating the Jak-Stat pathway in cardiomyocytes

Mutsuo Harada[1,4], Yingjie Qin[1,4], Hiroyuki Takano[1,4], Tohru Minamino[1,4], Yunzeng Zou[1], Haruhiro Toko[1], Masashi Ohtsuka[1], Katsuhisa Matsuura[1], Masanori Sano[1], Jun-ichiro Nishi[1], Koji Iwanaga[1], Hiroshi Akazawa[1], Takeshige Kunieda[1], Weidong Zhu[1], Hiroshi Hasegawa[1], Keita Kunisada[2], Toshio Nagai[1], Haruaki Nakaya[3], Keiko Yamauchi-Takihara[2] & Issei Komuro[1]

Granulocyte colony-stimulating factor (G-CSF) was reported to induce myocardial regeneration by promoting mobilization of bone marrow stem cells to the injured heart after myocardial infarction, but the precise mechanisms of the beneficial effects of G-CSF are not fully understood. Here we show that G-CSF acts directly on cardiomyocytes and promotes their survival after myocardial infarction. G-CSF receptor was expressed on cardiomyocytes and G-CSF activated the Jak/Stat pathway in cardiomyocytes. The G-CSF treatment did not affect initial infarct size at 3 d but improved cardiac function as early as 1 week after myocardial infarction. Moreover, the beneficial effects of G-CSF on cardiac function were reduced by delayed start of the treatment. G-CSF induced antiapoptotic proteins and inhibited apoptotic death of cardiomyocytes in the infarcted hearts. G-CSF also reduced apoptosis of endothelial cells and increased vascularization in the infarcted hearts, further protecting against ischemic injury. All these effects of G-CSF on infarcted hearts were abolished by overexpression of a dominant-negative mutant Stat3 protein in cardiomyocytes. These results suggest that G-CSF promotes survival of cardiac myocytes and prevents left ventricular remodeling after myocardial infarction through the functional communication between cardiomyocytes and noncardiomyocytes.

Myocardial infarction is the most common cause of cardiac morbidity and mortality in many countries, and left ventricular remodeling after myocardial infarction is important because it causes progression to heart failure. Several cytokines including G-CSF, erythropoietin and leukemia inhibitory factor have beneficial effects on cardiac remodeling after myocardial infarction[1–5]. In particular, G-CSF markedly improves cardiac function and reduce mortality after myocardial infarction in mice, possibly by regeneration of myocardium and angiogenesis[1,2,6–8]. G-CSF is known to have various functions such as induction of proliferation, survival and differentiation of hematopoietic cells, as well as mobilization of bone marrow cells[9–11]. Although it was reported that bone marrow cells could differentiate into cardiomyocytes and vascular cells, thereby contributing to regeneration of myocardium and angiogenesis in ischemic hearts[12–15], accumulating evidence has questioned these previous reports[16–18]. In this study, we examined the molecular mechanisms of how G-CSF prevents left ventricular remodeling after myocardial infarction.

RESULTS

G-CSF directly acts on cultured cardiomyocytes

G-CSF receptor (G-CSFR, encoded by *CSF3R*) has been reported to be expressed only on blood cells such as myeloid leukemic cells, leukemic cell lines, mature neutrophils, platelets, monocytes and some lymphoid cell lines[9]. To test whether G-CSFR is expressed on mouse cardiomyocytes, we performed a reverse transcription–polymerase chain reaction (RT-PCR) experiment by using specific primers for mouse *Csf3r*. We detected expression of the *Csf3r* gene in the adult mouse heart and cultured neonatal cardiomyocytes (**Fig. 1a**). We next examined expression of G-CSFR protein in cultured cardiomyocytes of neonatal rats by immunocytochemistry. Similar to the previously reported expression pattern of G-CSFR in living cells[19], the immunoreactivity for G-CSFR was localized to the cytoplasm and cell membrane under steady-state conditions in cardiomyocytes (**Fig. 1b**). This immunoreactivity disappeared when the antibody specific for G-CSFR was omitted, validating its specificity (**Fig. 1b**). In addition to cardiomyocytes, we also detected expression of G-CSFR on cardiac fibroblasts by immunocytochemistry (see **Supplementary Fig. 1** online) and RT-PCR (**Supplementary Fig. 2** online).

The binding of G-CSF to its receptor has been reported to evoke signal transduction by activating the receptor-associated Janus family tyrosine kinases (JAK) and signal transducer and activator of transcription (STAT) proteins in hematopoietic cells[9,10]. In particular, STAT3

[1]Department of Cardiovascular Science and Medicine, Chiba University Graduate School of Medicine, 1-8-1 Inohana, Chuo-ku, Chiba 260-8670, Japan. [2]Department of Molecular Medicine, Osaka University Medical School, Osaka University, 2-2 Yamadaoka, Suita, Osaka 565-0871, Japan. [3]Department of Pharmacology, Chiba University Graduate School of Medicine, 1-8-1 Inohana, Chuo-ku, Chiba 260-8670, Japan. [4]These authors contributed equally to this work. Correspondence should be addressed to I.K. (komuro-tky@umin.ac.jp).

Published online 20 February 2005; doi:10.1038/nm1199

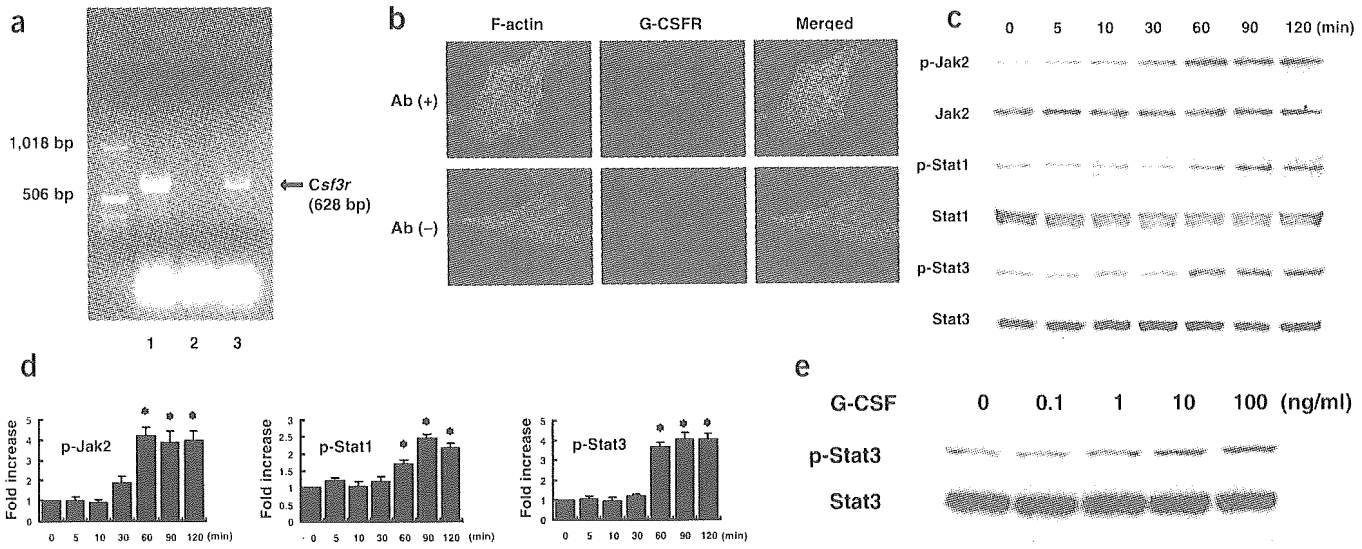

Figure 1 Expression of G-CSFR and the G-CSF-evoked signal transduction in cultured cardiomyocytes. (**a**) RT-PCR for mouse *Csf3r*. Expression of *Csf3r* was detected in the adult mouse heart (lane 1) and cultured cardiomyocytes of neonatal mice (lane 3). In lane 2, reverse transcription products were omitted to exclude the possibility of false-positive results from contamination. (**b**) Immunocytochemical staining for G-CSFR. Cardiomyocytes from neonatal rats were incubated with antibody to G-CSFR (red) and phalloidin (green) (upper panel). In the absence of antibody to G-CSFR, no signal was detected (lower panel). Original magnification, ×1,000. (**c**) G-CSF induces phosphorylation of Jak2, Stat1 and Stat3 in a time-dependent manner in cultured cardiomyocytes. (**d**) Quantification of Jak2, Stat1 and Stat3 activation by G-CSF stimulation as compared with control (time = 0). $^{*}P < 0.05$ versus control ($n = 3$). (**e**) G-CSF induces phosphorylation and activation of Stat3 in a dose-dependent manner in cultured cardiomyocytes.

has been reported to contribute to G-CSF-induced myeloid differentiation and survival[20,21]. We therefore examined whether G-CSF activates the Jak-Stat signaling pathway in cultured cardiomyocytes. G-CSF (100 ng/ml) significantly induced phosphorylation and activation of Jak2 and Stat3, and to a lesser extent, Stat1 but not Jak1, Tyk2 or Stat5 in a dose-dependent manner (**Fig. 1c–e** and data not shown), suggesting that G-CSFR on cardiomyocytes is functional.

We next examined whether G-CSF confers direct protective effects on cardiomyocytes as it prevents hematopoietic cells from apoptotic death[21]. We exposed cardiomyocytes to 0.1 mM H_2O_2 in the absence or presence of G-CSF and examined cardiomyocyte apoptosis by staining with annexin V[22,23]. Pretreatment with G-CSF significantly reduced the number of H_2O_2-induced annexin V–positive cells compared with cells that were not given the G-CSF pretreatment

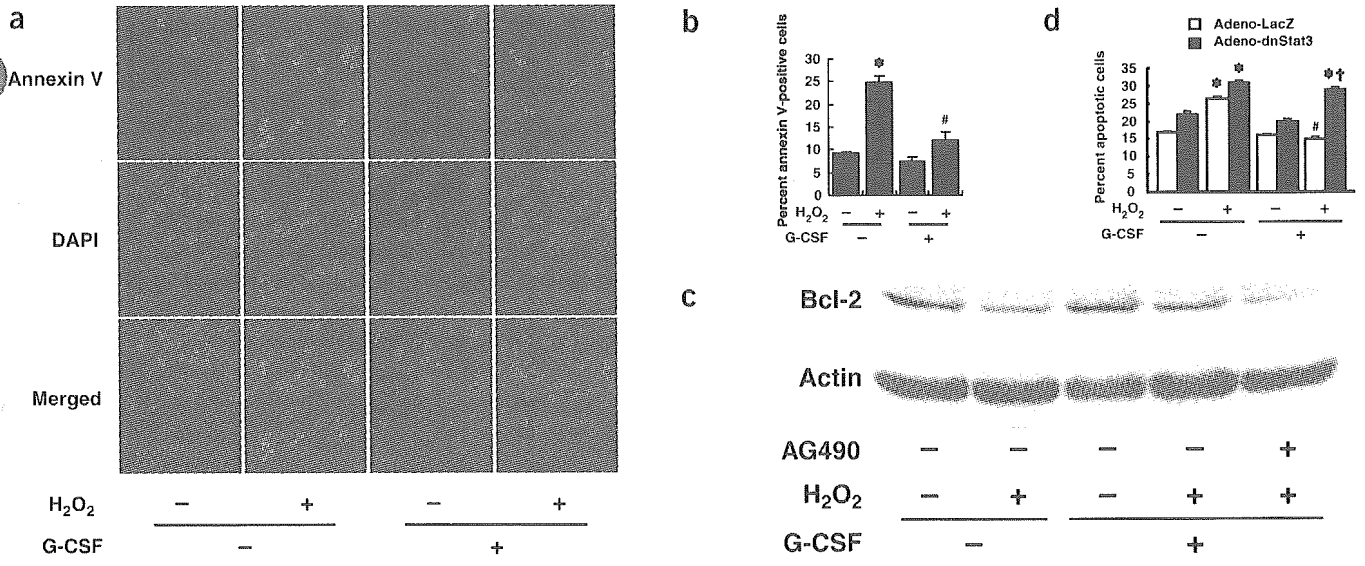

Figure 2 Suppression of H_2O_2-induced cardiomyocyte apoptosis by G-CSF. (**a**) Detection of apoptosis by Cy3-labeled annexin V. Red fluorescence shows apoptotic cardiomyocytes stained with Cy3-labeled annexin V. Nuclei were counterstained with DAPI staining (blue). Original magnification, ×400. (**b**) Quantitative analysis of apoptotic cells. The vertical axis indicates the ratio of the annexin V–positive cell number relative to that of DAPI-positive nuclei. $^{*}P < 0.01$ versus nontreated cells, $^{\#}P < 0.05$ versus H_2O_2-treated cells without G-CSF ($n = 3$). (**c**) G-CSF prevents H_2O_2-induced downregulation of Bcl-2 expression ($n = 3$). (**d**) Inhibition of antiapoptotic effects of G-CSF by Adeno-dnStat3. Bar graphs represent quantitative analysis of the apoptotic cell number relative to the total cell number. $^{*}P < 0.001$ versus H_2O_2 (−)/G-CSF (−), $^{\#}P < 0.001$ versus H_2O_2 (+)/G-CSF (−), $^{\dagger}P < 0.001$ versus H_2O_2 (+)/G-CSF (+)/Adeno-LacZ ($n = 3$).

(**Fig. 2a,b**). To investigate the molecular mechanism of how G-CSF exerts an antiapoptotic effect on cultured cardiomyocytes, we examined expression of the Bcl-2 protein family, known target molecules of the Jak-Stat pathway[24], by western blot analysis. Expression levels of antiapoptotic proteins such as Bcl-2 and Bcl-xL were lower when cardiomyocytes were subjected to H_2O_2 (**Fig. 2c** and data not shown), and this reduction was considerably inhibited by G-CSF pretreatment (**Fig. 2c**). AG490, an inhibitor of Jak2, abolished G-CSF-induced Bcl-2 expression (**Fig. 2c**) but did not affect its basal levels (**Supplementary Fig. 3** online), suggesting a crucial role of the Jak-Stat pathway in inducing survival of cardiomyocytes by G-CSF. To further elucidate the involvement of the Jak-Stat pathway in the protective effects of G-CSF on cardiomyocytes, we transduced cultured cardiomyocytes with adenovirus encoding dominant-negative Stat3 (Adeno-dnStat3). G-CSF treatment significantly reduced apoptosis induced by H_2O_2 in Adeno-LacZ-infected cardiomyocytes (**Fig. 2d**). This effect was abolished by introduction of Adeno-dnStat3 (**Fig. 2d**), suggesting that Stat3 mediates the protective effects of G-CSF on H_2O_2-induced cardiomyocyte apoptosis.

Effects of G-CSF on cardiac function after myocardial infarction

Consistent with the *in vitro* data, G-CSF enhanced activation of Stat3 in the infarcted heart (**Fig. 3a**). Notably, the levels of G-CSFR were markedly increased after myocardial infarction in cardiomyocytes (**Supplementary Fig. 4** online), which may enhance the effects of G-CSF on the infarcted heart. To elucidate the role of G-CSF-induced Stat3 activation in cardiac remodeling, we produced myocardial infarction in transgenic mice which express dominant-negative Stat3 in cardiomyocytes under the control of the α-myosin heavy chain promoter (dnStat3-Tg). Administration of G-CSF was started at the time of coronary artery ligation (day 0) until day 4 in transgenic mice; we termed this group Tg-G mice. A control group of dnStat3-Tg mice given myocardial infarction received saline (Tg-cont) instead of G-CSF. We also included two groups of wild-type mice given myocardial infarction treated with G-CSF (Wt-G) or saline (Wt-cont). At 2 weeks after myocardial infarction, we assessed the morphology by histological analysis and measured cardiac function by echocardiography and catheterization analysis. The infarct area was significantly smaller in the Wt-G group than the Wt-cont group (**Fig. 3b**). The Wt-G group also showed less left ventricular end-diastolic dimension (LVEDD) and better fractional shortening as assessed by echocardiography, and lower end-diastolic pressure (LVEDP) and better $+dp/dt$ and $-dp/dt$ as assessed by cardiac catheterization compared with Wt-cont (**Fig. 3c**). The beneficial effects of G-CSF on cardiac function were dose dependent and were significantly reduced by delayed start of the treatment (**Fig. 3d,e** and **Supplementary Fig. 5** online). Moreover, its favorable effects on cardiac function became evident within 1 week after the treatment (**Fig. 3f**). Disruption of the Stat3 signaling pathway in cardiomyocytes abolished the protective effects of G-CSF. There was no significant difference in LVEDD, fractional shortening, LVEDP, $+dp/dt$ and $-dp/dt$ between Tg-G and Tg-cont (**Fig. 3c**). We obtained similar results from infarcted female hearts (**Fig. 3g**). These results suggest that G-CSF protects the heart after myocardial infarction at least in part by directly activating Stat3 in cardiomyocytes, which is a gender-independent effect. We have previously shown that treatment with G-CSF significantly ($P < 0.05$) decreased myocardial infarction–related mortality of wild-type mice[2]. In contrast, there were no significant differences in mortality between G-CSF-treated and saline-treated dnStat3-Tg mice (data not shown).

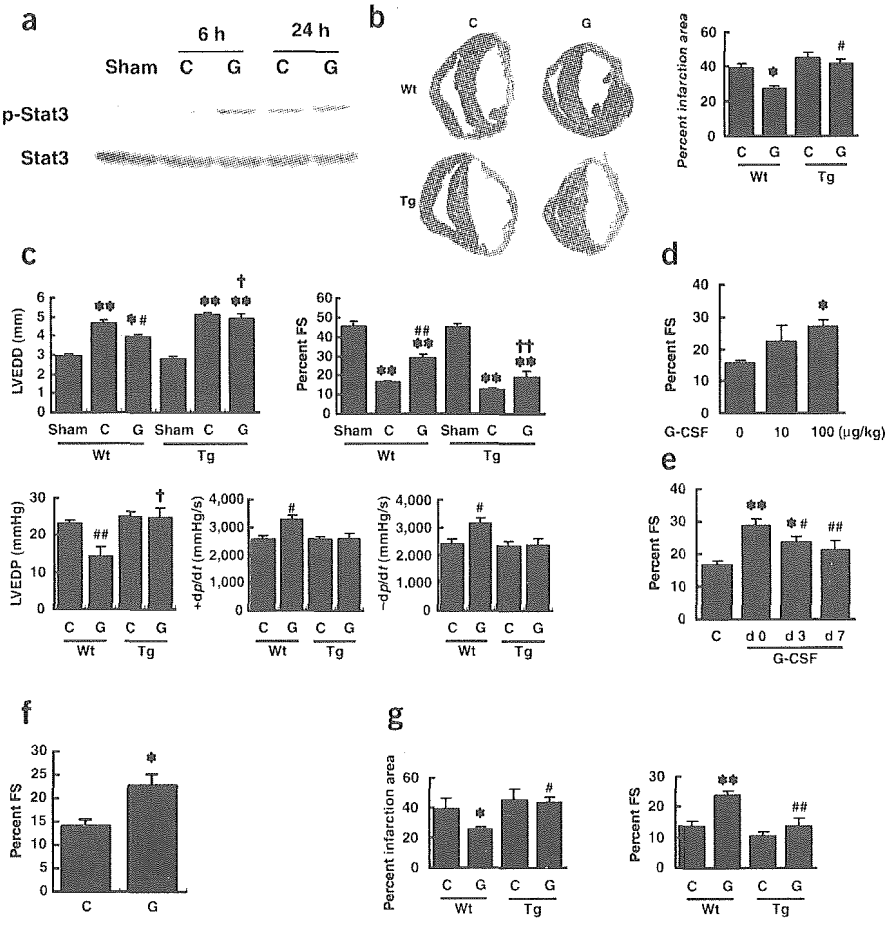

Figure 3 Effects of G-CSF on cardiac function after myocardial infarction. (**a**) Stat3 activation in the infarcted hearts. We operated on wild-type mice to induce myocardial infarction and treated them with G-CSF (G) or saline (C). (**b**) Masson trichrome staining of wild-type (Wt) and dnStat3-Tg (Tg) hearts. $^{*}P < 0.001$ versus Wt-cont, $^{\#}P < 0.001$ versus Wt-G ($n = 11$–15). (**c**) G-CSF treatment preserves cardiac function after myocardial infarction. $^{*}P < 0.01$, $^{**}P < 0.001$ versus sham; $^{\#}P < 0.05$, $^{\#\#}P < 0.001$ versus Wt-cont; $^{\dagger}P < 0.01$, $^{\dagger\dagger}P < 0.001$ versus Wt-G ($n = 10$–15 for echocardiography and $n = 5$ for catheterization analysis). (**d**) Dose-dependent effects of G-CSF. FS, *fractional shortening*. $^{*}P < 0.01$ *versus* saline-treated mice (G-CSF = 0)($n = 12$–14). (**e**) Wild-type mice were operated to induce myocardial infarction and G-CSF treatment (100 μg/kg/d) was started from the indicated day for 5 d. $^{*}P < 0.05$, $^{**}P < 0.001$ versus saline-treated mice (C); $^{\#}P < 0.05$, $^{\#\#}P < 0.01$ versus mice treated at day 0 (d 0) ($n = 11$–12). (**f**) Effects of G-CSF on cardiac function at 1 week. $^{*}P < 0.05$ versus control ($n = 3$). (**g**) Effects of G-CSF on cardiac function of female mice. $^{*}P < 0.05$, $^{**}P < 0.001$ versus Wt-cont; $^{\#}P < 0.05$, $^{\#\#}P < 0.005$ versus Wt-G ($n = 4$–5).

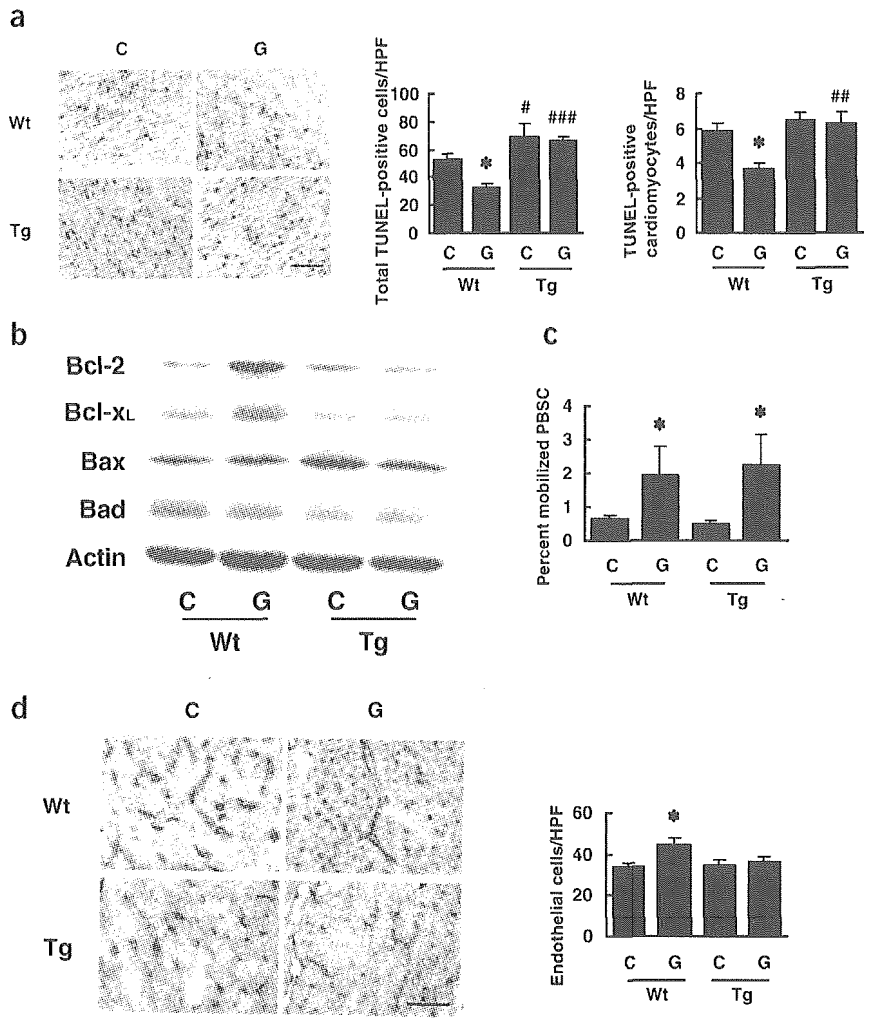

Figure 4 Mechanisms of the protective effects of G-CSF. (**a**) TUNEL staining (brown nuclei) in the infarcted hearts. The graphs show quantitative analyses for total TUNEL-positive cells (left graph) and TUNEL-positive cardiomyocytes (right graph) in infarcted hearts. $^{*}P < 0.01$ versus Wt-cont; $^{\#}P < 0.05$, $^{\#\#}P < 0.005$, $^{\#\#\#}P < 0.001$ versus wild-type mice with the same treatment ($n = 5$–7). Scale bar, 100 μm. (**b**) Infarcted hearts treated with G-CSF (G) or saline (C) were analyzed for expression of Bcl-2, Bcl-xL, Bax and Bad by western blotting ($n = 3$). (**c**) Mobilization of hematopoietic stem cells into peripheral blood (PBSC). $^{*}P < 0.05$ versus saline-treated mice ($n = 4$). (**d**) Capillary endothelial cells were identified by immunohistochemical staining with anti-PECAM antibody in the border zone of the infarcted hearts. Scale bar, 100 μm. The number of endothelial cells was counted and shown in the graph ($n = 6$–8). $^{*}P < 0.05$.

Mechanisms of the protective effects of G-CSF

Our *in vitro* results suggest that the protective effects of G-CSF on cardiac remodeling after myocardial infarction can be attributed in part to reduction of cardiomyocyte apoptosis. To determine whether the Stat3 pathway in cardiomyocytes mediates the antiapoptotic effects of G-CSF on the ischemic myocardium, we carried out TUNEL labeling of left ventricular sections 24 h after myocardial infarction in wild-type mice and dnStat3-Tg mice. Although the number of TUNEL-positive cells was significantly less in the Wt-G group than the Wt-cont group, G-CSF treatment had no effect on cardiomyocyte apoptosis in dnStat3-Tg mice (**Fig. 4a**). The effects of G-CSF on apoptosis after myocardial infarction were also attenuated when mice were treated with AG490 (**Supplementary Fig. 6** online). Myocardial infarction–related apoptosis was significantly increased in the Tg-cont group and AG490-treated wild-type mice compared with Wt-cont mice (**Fig. 4a** and **Supplementary Fig. 6** online), suggesting that endogenous activation of Stat3 has a protective role in the infarcted heart, as reported previously[25]. It is noteworthy that G-CSF treatment inhibited apoptosis of noncardiomyocytes including endothelial cells and that this inhibition was abolished in dnStat3-Tg mice (**Fig. 4a** and data not shown). To investigate the underlying molecular mechanism of the antiapoptotic effects of G-CSF *in vivo*, we examined expression of the Bcl-2 protein family by western blot analysis. Consistent with our *in vitro* results, expression of antiapoptotic proteins such as Bcl-2 and Bcl-xL was significantly increased in the Wt-G group at 24 h after myocardial infarction compared with the Wt-cont group, whereas expression of the proapoptotic proteins Bax and Bad was not affected by the treatment (**Fig. 4b**). In contrast, expression levels of antiapoptotic proteins were not increased by G-CSF in the Tg-G group (**Fig. 4b**). Immunohistochemical analysis also showed increased expression of Bcl-2 in the infarcted heart of the Wt-G group but not of the Tg-G group (**Supplementary Fig. 7** online).

To determine the effects of G-CSF on mobilization of stem cells, we counted the number of cells positive for both Sca-1 and c-kit in peripheral blood samples from mice treated with G-CSF or saline. The G-CSF treatment similarly increased the number of double-positive cells in wild-type mice and dnStat3-Tg mice (**Fig. 4c**). To examine the impact of G-CSF on cardiac homing of bone marrow cells, we transplanted bone marrow cells derived from GFP transgenic mice into wild-type and dnStat3-Tg mice, produced myocardial infarction and treated with G-CSF or saline. FACS analysis showed that G-CSF did not increase cardiac homing of bone marrow cells in wild-type and dnStat3-Tg mice (**Supplementary Fig. 8** online). We have shown that cardiac stem cells, which are able to differentiate into cardiomyocytes, exist in Sca-1-positive populations in the adult myocardium[26]. But G-CSF treatment did not affect the number of Sca-1-positive cells in the infarcted hearts of wild-type or dnStat3-Tg mice (**Supplementary Fig. 9** online). Thus, it is unlikely that G-CSF exerts its beneficial effects through expansion of cardiac stem cells. To determine the effects of G-CSF on proliferation of cardiomyocytes, we carried out immunostaining for Ki67, a marker for cell cycling, in conjunction with a labeling for troponin T. The number of Ki67-positive cardiomyocytes was increased in the infarcted hearts of wild-type mice and dnStat3-Tg mice compared with sham-operated mice (**Supplementary Fig. 10** online). But G-CSF did not alter the number of Ki67-positive cardiomyocytes in wild-type or dnStat3-Tg mice, suggesting that G-CSF does not induce proliferation of cardiomyocytes (**Supplementary Fig. 10** online). The number of Ki67-positive cardiomyocytes was less in infarcted hearts of dnStat3-Tg mice than in those of wild-type mice, suggesting that endogenous Stat3 activity is required

for myocardial regeneration after myocardial infarction and that activation of Stat3 by G-CSF is not sufficient for cardiomyocytes to enter the cell cycle in infarcted hearts of wild-type mice (**Supplementary Fig. 10** online). In contrast, G-CSF treatment significantly increased the number of endothelial cells in the border zone of the infarcted hearts (**Fig. 4d**). This increase was attenuated in dnStat3-Tg mice, indicating that the increased vascularity is mediated by Stat3 activity in cardiomyocytes and may partially account for the beneficial effects of G-CSF on the infarcted hearts. Taken together with the result that G-CSF-induced inhibition of noncardiomyocyte apoptosis was also mediated by the Stat3 signaling pathway in cardiomyocytes (**Fig. 4a**), these findings imply that communication between cardiomyocytes and noncardiomyocytes regulates each others' survival.

To further test whether G-CSF acts directly on the heart, we examined the effects of G-CSF treatment on cardiac function after ischemia-reperfusion injury in a Langendorff perfusion model. The isolated hearts underwent 30 min total ischemia followed by 120 min reperfusion with the perfusate containing G-CSF (300 ng/ml) or vehicle, and left ventricular developed pressure (LVDP, measured as the difference between systolic and diastolic pressures of the left ventricle) and LVEDP were measured. There were no significant differences in basal hemodynamic parameters including heart rate, left ventricular pressure, LVEDP and positive and negative d*p*/d*t*, between the control group and G-CSF group (**Table 1**). After reperfusion, however, G-CSF-treated hearts started to beat earlier than those of the control group (**Fig. 5a**). At 120 min after reperfusion, contractile function (LVDP) of G-CSF-treated hearts was significantly better than that of control hearts (**Fig. 5a**). Likewise, diastolic function (LVEDP) of G-CSF-treated hearts was better than that of control hearts (**Fig. 5a**). After ischemia-reperfusion, there was more viable myocardium (red lesion) in G-CSF-treated hearts than control hearts (**Fig. 5b**). The size of the infarct (white lesion) was significantly smaller in G-CSF-treated hearts than in control hearts (**Fig. 5b**).

Table 1 Basal hemodynamic parameters

	Control ($n = 7$)	G-CSF ($n = 7$)
HR (b.p.m.)	326 ± 34	334 ± 24
LVP (mmHg)	121.8 ± 24	117.3 ± 32
LVEDP (mmHg)	4.3 ± 1.3	4.5 ± 1.6
+d*p*/d*t* (mmHg/s)	7,554 ± 643	7,657 ± 377
−d*p*/d*t* (mmHg/s)	6,504 ± 638	6,670 ± 602

HR, heart rate; b.p.m., beats per minute; LVP, left ventricular pressure; LVEDP, left ventricular end-diastolic pressure; +d*p*/d*t* and −d*p*/d*t*, positive and negative first derivatives for maximal rates of left ventricular pressure development.

DISCUSSION

In the present study, G-CSFR was found to be expressed on cardiomyocytes and cardiac fibroblasts, and G-CSF activated Jak2 and the downstream signaling molecule Stat3 in cultured cardiomyocytes. Treatment with G-CSF protected cultured cardiomyocytes from apoptotic cell death possibly through upregulation of Bcl-2 and Bcl-xL expression, suggesting that G-CSF has direct protective effects on cardiomyocytes through G-CSFR and the Jak-Stat pathway. This idea is further supported by the *in vivo* experiments. G-CSF enhanced Stat3 activity and increased expression of Bcl-2 and Bcl-xL in the infarcted heart where G-CSFR was markedly upregulated, thereby preventing cardiomyocyte apoptosis and cardiac dysfunction. These effects of G-CSF were abolished when Stat3 activation was disrupted in cardiomyocytes, suggesting that a direct action of G-CSF on cardiomyocytes has a crucial role in preventing left ventricular remodeling after myocardial infarction. Because noncardiomyocytes also expressed G-CSFR, the possibility exists that activation of G-CSF receptors on these cells modulates the beneficial effects of G-CSF on infarcted hearts.

The mobilization of bone marrow stem cells (BMSC) to the myocardium has been considered to be the main mechanism by which G-CSF ameliorates cardiac remodeling after myocardial infarction[1,6–8]. In this study, we showed that G-CSF reduces apoptotic cell death and effectively protects the infarcted heart, which is dependent on its direct action on cardiomyocytes through the Stat3 pathway. This antiapoptotic mechanism seems to be more important than induction of BMSC mobilization, because disruption of

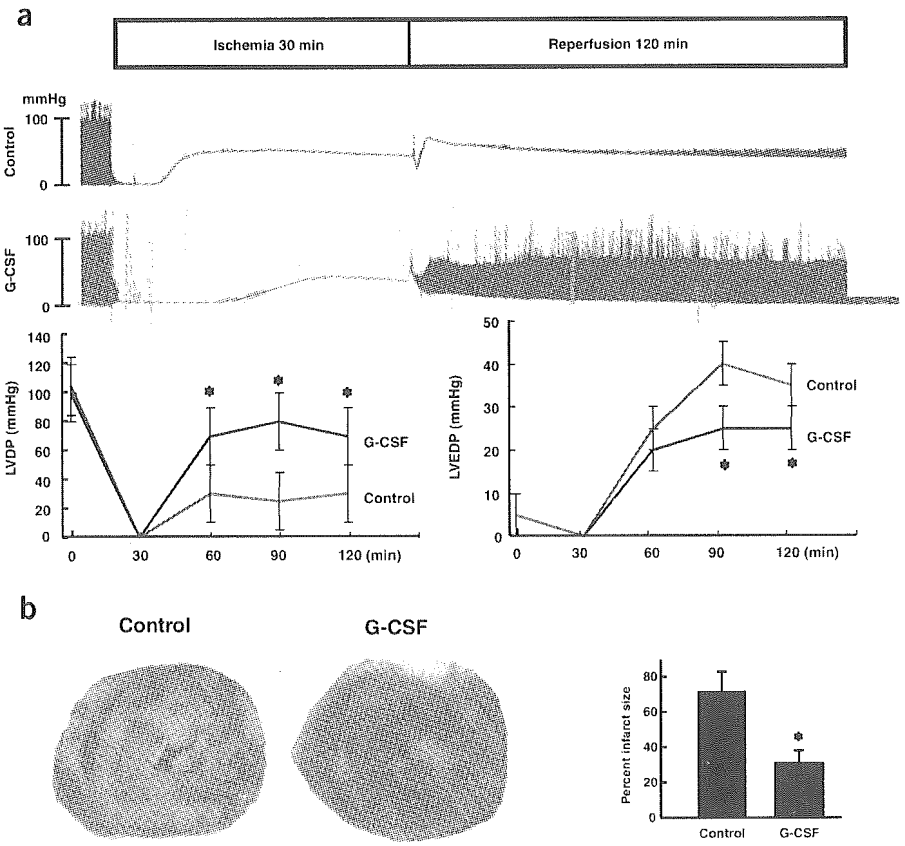

Figure 5 Direct effects of G-CSF on cardiac function after ischemia-reperfusion injury. (**a**) Representative left ventricular pressure records of control and G-CSF-treated hearts are shown (upper panel). The graphs show changes in LVDP (left) and LVEDP (right) during ischemia-reperfusion. $^*P < 0.05$ versus control hearts ($n = 7$). (**b**) The photographs show representative TTC staining of control hearts (Control) and G-CSF-treated hearts (G-CSF) after ischemia-reperfusion. The graph indicates myocardial infarct sizes for control hearts (Control) and G-CSF-treated hearts (G-CSF). Infarct sizes were calculated as described in **Supplementary Methods** online. $^*P < 0.05$ versus control hearts ($n = 7$).

this pathway by expressing dnStat3 in cardiomyocytes almost abolished the protective effects of G-CSF on cardiac remodeling after myocardial infarction. In addition, there was no difference in the effects of G-CSF on mobilization and cardiac homing of bone marrow cells, expansion of cardiac stem cells, and proliferation of cardiomyocytes between wild-type and dnStat3-Tg mice. The beneficial effects of G-CSF and stem cell factor on the infarcted heart has been described, but no evidence indicating that G-CSF induced cardiac homing of bone marrow cells in the infarcted heart has been shown[1]. In this study, we found favorable effects of G-CSF on the infarcted heart as early as 1 week after the treatment even though cardiac homing of bone marrow cells was not increased. Thus, we conclude that increased cardiac homing of bone marrow cells cannot account for improved function of the infarcted heart after G-CSF treatment.

The JAK-STAT pathway has been shown to induce various angiogenic factors besides antiapoptotic proteins[20,21]. The number of endothelial cells in the border zone was increased by G-CSF through Stat3 activation in cardiomyocytes. Consistent with this, we noted that G-CSF induces cardiac expression of angiogenic factors *in vitro* and *in vivo*, which appears to be mediated by cardiac Stat3 activation (M.H., Y.Q., H.T., T.M. & I.K., unpublished data). Moreover, we observed that the majority of apoptotic cells in the infarcted hearts was endothelial cells and that endothelial apoptosis was significantly inhibited by G-CSF treatment in wild-type mice but not in dnStat3-Tg mice (**Fig. 4a** and M.H., T.M. & I.K., unpublished data). Thus, activation of this pathway in cardiomyocytes by G-CSF may also promote angiogenesis and protect against endothelial apoptosis by producing angiogenic factors, resulting in the further prevention of cell death of cardiomyocytes and cardiac remodeling after myocardial infarction. The results in this study provide new mechanistic insights of the G-CSF therapy on infarcted hearts.

METHODS

For further details, please see **Supplementary Methods** online.

Cell culture. Cardiomyocytes prepared from ventricles of 1-d-old Wistar rats[27] were plated onto 60-mm plastic culture dishes at a concentration of 1×10^5 cells/cm^2 and cultured in Dulbecco modified Eagle medium (DMEM) supplemented with 10% fetal bovine serum (FBS) at 37 °C in a mixture of 95% air and 5% CO_2. The culture medium was changed to serum-free DMEM 24 h before stimulation. Generation and infection of recombinant adenovirus were performed as described[28].

Percoll enrichment of adult mouse cardiomyocytes and noncardiomyocytes. Adult mouse cardiomyocytes were prepared from 10-week-old C57BL/6 male mice according to the Alliance for Cellular Signaling protocol. We also prepared cardiomyocytes and noncardiomyocytes from myocardial infarction-operated or sham-operated C57BL/6 male mice. After digestion, cells were dissociated, resuspended in differentiation medium and loaded onto a discontinuous Percoll gradient. Cardiomyocytes or noncardiomyocytes were separately collected as described previously[29] and subsequently washed with 1 × phosphate-buffered saline for RT-PCR.

RNA extraction and RT-PCR analysis. Total RNA from adult mice cardiomyocytes was isolated by the guanidinium thiocyanate-phenol chloroform method. A total of 4 μg RNA was transcribed with MMLV reverse transcriptase and random hexamers. The cDNA was amplified using a mouse *Csf3r* exon 15 forward primer (5′-GTACTCTTGTCCACTACCTGT-3′) and an exon 17 reverse primer (5′-CAAGATACAAGGACCCCCAA-3′). We performed PCR under the following conditions: an initial denaturation at 94 °C for 2 min followed by a cycle of denaturation at 94 °C for 1 min, annealing at 58 °C for 1 min and extension at 72 °C for 1 min. We subjected samples to 40 cycles followed by a final extension at 72 °C for 3 min. The products were analyzed on a 1.5% ethidium bromide stained agarose gel.

Immunocytochemistry. Cardiomyocytes or noncardiomyocytes of neonatal rats cultured on glass cover slips were incubated with or without the antibody to G-CSFR (Santa Cruz Biotechnology) for 1 h, followed by incubation with Cy3-labeled secondary antibodies. After washing, we double-stained the cells with fluorescent phalloidin (Molecular Probes) for 1 h at room temperature.

Western blots. Western blot analysis was performed as described[5]. We probed the membranes with antibodies to phospho-Jak2, phospho-Stat3 (Cell Signaling), phospho-Jak1, phospho-Tyk2, phospho-Stat1, phospho-Stat5, anti-Jak1, Jak2, Tyk2, Stat1, Stat3, Stat5, Bcl-2, Bax, G-CSFR (Santa Cruz Biotechnology), Bcl-xL, Bad (Transduction Laboratories) or actin (Sigma-Aldrich). We used the ECL system (Amersham Biosciences Corp) for detection.

Animals and surgical procedures. Generation and genotyping of dnStat3-Tg mice have been previously described[28]. All mice used in this study were 8–10-week-old males, unless indicated. All experimental procedures were performed according to the guidelines established by Chiba University for experiments in animals and all protocols were approved by our institutional review board. We anesthetized mice by intraperitoneally injecting a mixture of 100 mg/kg ketamine and 5 mg/kg xylazine. Myocardial infarction was produced by ligation of the left anterior descending artery. We operated on dnStat3-Tg mice to induce myocardial infarction and randomly divided them into two groups, the G-CSF-treated group (10–100 μg/kg/d subcutaneously for 5 d consecutively, Kyowa Hakko Kogyo Co.) and the saline-treated group. We operated on nontransgenic mice as control groups using the same procedures and divided them into a G-CSF-treated group and a saline-treated group. Some mice were randomly chosen to be analyzed for initial area at risk by injection of Evans blue dye after producing myocardial infarction. There was no difference in initial area sizes at risk between saline-treated control and G-CSF-treated mice ($n = 5$; **Supplementary Fig. 11** online). We also determined initial infarct size by triphenyltetrazolium chloride staining on day 3. There was no significant difference in initial infarct size between saline-treated control and G-CSF-treated mice ($n = 5$; **Supplementary Fig. 12** online).

Echocardiography and catheterization. Transthoracic echocardiography was performed with an Agilent Sonos 4500 (Agilent Technology Co.) provided with an 11-MHz imaging transducer. For catheterization analysis, the right carotid artery was cannulated under anesthesia by the micro pressure transducers with an outer diameter of 0.42 mm (Samba 3000; Samba Sensors AB), which was then advanced into the left ventricle. Pressure signals were recorded using a MacLab 3.6/s data acquisition system (AD Instruments) with a sampling rate of 2,000 Hz. Mice were anesthetized as described above, and heart rate was kept at approximately 270–300 beats per minute to minimize data deviation when we measured cardiac function.

Histology. Hearts fixed in 10% formalin were embedded in paraffin, sectioned at 4 μm thickness, and stained with Masson trichrome. The extent of fibrosis was measured in three sections from each heart and the value was expressed as the ratio of Masson trichrome stained area to total left ventricular free wall. For apoptosis analysis, infarcted hearts were frozen in cryomolds, sectioned, and TUNEL labeling was performed according to the manufacturer's protocol (*In Situ* Apoptosis Detection kit; Takara) in combination with immunostainings for appropriate cell markers. Digital photographs were taken at magnification ×400, and 25 random high-power fields (HPF) from each heart sample were chosen and quantified in a blinded manner. We examined vascularization by measuring the number of capillary endothelial cells in light-microscopic sections taken from the border zone of the hearts 2 weeks after myocardial infarction. Capillary endothelial cells were identified by immunohistochemical staining with antibody to platelet endothelial cell adhesion molecule (PECAM; Pharmingen). Ten random microscopic fields in the border zone were examined and the number of endothelial cells was expressed as the number of PECAM-positive cells/HPF (magnification, ×400).

Statistical analysis. Data are shown as mean ± s.e.m. Multiple group comparison was performed by one-way analysis of variance (ANOVA) followed by the Bonferroni procedure for comparison of means. Comparison between two groups were analyzed by the two-tailed Student's *t*-test or two-way ANOVA. Values of $P < 0.05$ were considered statistically significant.

URL. Alliance for Cellular Signaling Procedure Protocols
http://www.signaling-gateway.org/data/cgi-bin/Protocols.cgi?cat=0

Note: Supplementary information is available on the Nature Medicine website.

ACKNOWLEDGMENTS

The authors thank J. Robbins (Children's Hospital Research Foundation, Cincinnati, Ohio) for a fragment of the αMHC gene promoter, M. Tamagawa for the analysis of Langendorff-perfused model, Kirin Brewery Co., Ltd. for their kind gift of G-CSF, and M. Watanabe and E. Fujita for their technical assistance. This work was supported by a Grant-in-Aid for Scientific Research, Developmental Scientific Research, and Scientific Research on Priority Areas from the Ministry of Education, Science, Sports, and Culture and by the Program for Promotion of Fundamental Studies in Health Sciences of the Organization for Drug ADR Relief, R&D Promotion and Product Review of Japan (to I.K.) and Japan Research Foundation for Clinical Pharmacology (to T.M.).

COMPETING INTERESTS STATEMENTS

The authors declare that they have no competing financial interests.

Received 8 September 2004; accepted 19 January 2005
Published online at http://www.nature.com/naturemedicine/

1. Orlic, D. *et al.* Mobilized bone marrow cells repair the infarcted heart, improving function and survival. *Proc. Natl. Acad. Sci. USA* **98**, 10344–10349 (2001).
2. Ohtsuka, M. *et al.* Cytokine therapy prevents left ventricular remodeling and dysfunction after myocardial infarction through neovascularization. *FASEB J.* **18**, 851–853 (2004).
3. Moon, C. *et al.* Erythropoietin reduces myocardial infarction and left ventricular functional decline after coronary artery ligation in rats. *Proc. Natl. Acad. Sci. USA* **100**, 11612–11617 (2003).
4. Parsa, C.J. *et al.* A novel protective effect of erythropoietin in the infarcted heart. *J. Clin. Invest.* **112**, 999–1007 (2003).
5. Zou, Y. *et al.* Leukemia inhibitory factor enhances survival of cardiomyocytes and induces regeneration of myocardium after myocardial infarction. *Circulation* **108**, 748–753 (2003).
6. Minatoguchi, S. *et al.* Acceleration of the healing process and myocardial regeneration may be important as a mechanism of improvement of cardiac function and remodeling by postinfarction granulocyte colony-stimulating factor treatment. *Circulation* **109**, 2572–2580 (2004).
7. Adachi, Y. *et al.* G-CSF treatment increases side population cell infiltration after myocardial infarction in mice. *J. Mol. Cell. Cardiol.* **36**, 707–710 (2004).
8. Kawada, H. *et al.* Nonhematopoietic mesenchymal stem cells can be mobilized and differentiate into cardiomyocytes after myocardial infarction. *Blood* **104**, 3581–3587 (2004).
9. Avalos, B.R. Molecular analysis of the granulocyte colony-stimulating factor receptor. *Blood* **88**, 761–777 (1996).
10. Demetri, G.D. & Griffin, J.D. Granulocyte colony-stimulating factor and its receptor. *Blood* **78**, 2791–808 (1991).
11. Berliner, N. *et al.* Granulocyte colony-stimulating factor induction of normal human bone marrow progenitors results in neutrophil-specific gene expression. *Blood* **85**, 799–803 (1995).
12. Orlic, D. *et al.* Bone marrow cells regenerate infarcted myocardium. *Nature* **410**, 701–705 (2001).
13. Asahara, T. *et al.* Bone marrow origin of endothelial progenitor cells responsible for postnatal vasculogenesis in physiological and pathological neovascularization. *Circ. Res.* **85**, 221–228 (1999).
14. Kocher, A.A. *et al.* Neovascularization of ischemic myocardium by human bone-marrow-derived angioblasts prevents cardiomyocyte apoptosis, reduces remodeling and improves cardiac function. *Nat. Med.* **7**, 430–436 (2001).
15. Jackson, K.A. *et al.* Regeneration of ischemic cardiac muscle and vascular endothelium by adult stem cells. *J. Clin. Invest.* **107**, 1395–1402 (2001).
16. Balsam, L.B. *et al.* Haematopoietic stem cells adopt mature haematopoietic fates in ischaemic myocardium. *Nature* **428**, 668–673 (2004).
17. Murry, C.E. *et al.* Haematopoietic stem cells do not transdifferentiate into cardiac myocytes in myocardial infarcts. *Nature* **428**, 664–668 (2004).
18. Norol, F. *et al.* Influence of mobilized stem cells on myocardial infarct repair in a nonhuman primate model. *Blood* **102**, 4361–4368 (2003).
19. Aarts, L.H., Roovers, O., Ward, A.C. & Touw, I.P. Receptor activation and 2 distinct COOH-terminal motifs control G-CSF receptor distribution and internalization kinetics. *Blood* **103**, 571–579 (2004).
20. Benekli, M., Baer, M.R., Baumann, H. & Wetzler, M. Signal transducer and activator of transcription proteins in leukemias. *Blood* **101**, 2940–2954 (2003).
21. Smithgall, T.E. *et al.* Control of myeloid differentiation and survival by Stats. *Oncogene* **19**, 2612–2618 (2000).
22. Dumont, E.A. *et al.* Cardiomyocyte death induced by myocardial ischemia and reperfusion: measurement with recombinant human annexin-V in a mouse model. *Circulation* **102**, 1564–1568 (2000).
23. van Heerde, W.L. *et al.* Markers of apoptosis in cardiovascular tissues: focus on Annexin V. *Cardiovasc. Res.* **45**, 549–559 (2000).
24. Bromberg, J. Stat proteins and oncogenesis. *J. Clin. Invest.* **109**, 1139–1142 (2002).
25. El-Adawi, H. *et al.* The functional role of the JAK-STAT pathway in post-infarction remodeling. *Cardiovasc. Res.* **57**, 129–138 (2003).
26. Matsuura, K. *et al.* Adult cardiac Sca-1-positive cells differentiate into beating cardiomyocytes. *J. Biol. Chem.* **279**, 11384–11391 (2004).
27. Zou, Y. *et al.* Both Gs and Gi proteins are critically involved in isoproterenol-induced cardiomyocyte hypertrophy. *J. Biol. Chem.* **274**, 9760–9770 (1999).
28. Funamoto, M. *et al.* Signal transducer and activator of transcription 3 is required for glycoprotein 130-mediated induction of vascular endothelial growth factor in cardiac myocytes. *J. Biol. Chem.* **275**, 10561–10566 (2000).
29. Ikeda, K. *et al.* The effects of sarpogrelate on cardiomyocyte hypertrophy. *Life Sci.* **67**, 2991–2996 (2000).

D. Shichi
E.F. Kikkawa
M. Ota
Y. Katsuyama
A. Kimura
A. Matsumori
J.K. Kulski
T.K. Naruse
H. Inoko

The haplotype block, *NFKBIL1-ATP6V1G2-BAT1-MICB-MICA*, within the class III – class I boundary region of the human major histocompatibility complex may control susceptibility to hepatitis C virus-associated dilated cardiomyopathy

Key words:
dilated cardiomyopathy (DCM); hepatitis C virus (HCV); human leukocyte antigen region; hypertrophic cardiomyopathy (HCM); microsatellite; single nucleotide polymorphism (SNP)

Acknowledgments
We are grateful to Drs A. Hasegawa, R. Nagai, T. Izumi, N. Aoyama, K. Yamauchi-Takihara, Y. Sato, Y. Takatsu, S. Maruyama, E. Matsuyama, K. Nakamura, T. Ohe, Y. Sakai, H. Kotoura, M. Matsuzaki, and T. Yamamura for their contributions in clinical evaluation and blood sampling from patients with HCV-DCM or HCV-HCM. This study was supported by grants as follows: Japanese Ministry of Health and Welfare, Mitsui Life Social Welfare Foundation, and Tokai University, School of Medicine Research Aid 2002.

Abstract: Cardiomyopathy is a heart muscle disease with impaired stretch response that can result in severe heart failure and sudden death. A small proportion of hepatitis C virus (HCV)-infected patients may be predisposed to develop dilated cardiomyopathy (DCM) and hypertrophic cardiomyopathy (HCM). The molecular mechanisms involved in the predisposition remain unknown due in part to the lack of information on their genetic background. Because the human leukocyte antigen (HLA) region has a pivotal role in controlling the susceptibility to HCV-induced liver disease, we hypothesized that particular *HLA* alleles and/or non-*HLA* gene alleles within the human major histocompatibility complex (MHC) genomic region might control the predisposition to HCV-associated DCM (HCV-DCM) and/or HCV-associated HCM (HCV-HCM). Here, we present mapping results of the MHC-related susceptibility gene locus for HCV-associated cardiomyopathy by analyzing microsatellite and single nucleotide polymorphism markers. To delineate the susceptibility locus, we genotyped 44 polymorphic markers scattered across the entire MHC region in a total of 59 patients (21 HCV-DCM and 38 HCV-HCM) and 120 controls. We mapped HCV-DCM susceptibility to a non-*HLA* gene locus spanning from *NFKBIL1* to *MICA* gene loci within the MHC class III – class I boundary region. Our results showed that HCV-DCM was more strongly associated with alleles of the non-*HLA* genes rather than the *HLA* genes themselves. In addition, no significant association was found between the MHC markers and HCV-HCM. This marked difference in the MHC-related disease susceptibility for HCV-associated cardiomyopathy strongly suggests that the development of HCV-DCM and HCV-HCM is under the control of different pathogenic mechanisms.

Authors' affiliation:

D. Shichi[1,2],
E.F. Kikkawa[1],
M. Ota[3],
Y. Katsuyama[3],
A. Kimura[2,4],
A. Matsumori[5],
J.K. Kulski[1,6],
T.K. Naruse[1],
H. Inoko[1]

[1]Department of Basic Medical Science and Molecular Medicine, Tokai University School of Medicine, Isehara, Kanagawa, Japan

[2]Department of Molecular Pathogenesis, Medical Research Institute, Tokyo Medical and Dental University, Chiyoda-ku, Tokyo, Japan

[3]Department of Legal Medicine, Sinshu University School of Medicine, Matsumoto, Nagano, Japan

[4]Laboratory of Genome Diversity, School of Biomedical Science, Tokyo Medical and Dental University, Chiyoda-ku, Tokyo, Japan

[5]Department of Cardiovascular Medicine, Kyoto University Graduate School of Medicine, Sakyo-ku, Kyoto, Japan

[6]Center for Bioinformatics and Biological Computing, Murdoch University School of Information Technology, Murdoch, Western Australia, Australia

Correspondence to:
Hidetoshi Inoko, PhD, MD
Department of Basic Medical Science and Molecular Medicine
Tokai University School of Medicine
Bohseidai, Isehara
Kanagawa 259-1193
Japan
Tel.:
+81 463 93 1121x2312
Fax: +81 463 94 8884
e-mail: hinoko@is.icc.u-tokai.ac.jp

Received 3 March 2005, revised 24 May 2005, accepted for publication 30 May 2005

doi: 10.1111/j.1399-0039.2005.00457.x

Tissue Antigens 2005: **66:** 200–208
Printed in Singapore.

Hepatitis C virus (HCV) is a major pathogen of liver disease (1). It also infects various extrahepatic tissues (2) and causes clinical manifestations that do not originate from hepatopathy (3). The extrahepatic manifestation includes cardiomyopathy that is defined as a heart muscle disease with impaired stretch response that can result in heart failure and sudden death (4–7). Dilated cardiomyopathy (DCM) and hypertrophic cardiomyopathy (HCM) are two major clinical phenotypes of the HCV-associated cardiomyopathy. DCM is characterized by chamber dilation with contractile dysfunction. In contrast, HCM exhibits cardiac hypertrophy with diastolic ventricular failure. Not all of the patients infected with HCV develop cardiomyopathy, and there is a report showing DCM and HCM can be found in 5.7 and 6.6%, respectively, of random patients with positive HCV antibody (8).

This epidemiological study suggests that there may be predisposing factors in the virus and/or infected host, which affect the clinical outcome of viral pathogenesis. To date, it is not clear whether or not there are cardiotropic HCV strains, and how they can escape cellular immune responses. It also remains unknown which genetic factors would predispose the infected patients to develop HCV-associated DCM (HCV-DCM) or HCV-associated HCM (HCV-HCM).

Human major histocompatibility complex (MHC), also called human leukocyte antigen (HLA) complex, on chromosome 6p21.3 plays a pivotal role in antiviral defense as a genetic factor controlling the immune response (9). The MHC genomic region consists of densely packed gene clusters including the *HLA* genes (10), the most polymorphic genes in the human genome (11–13). In addition to the classical and non-classical *HLA* class I and class II genes that regulate the cell-mediated immune response, there are at least 126 non-*HLA* coding genes within the MHC genomic region, which might affect acute and/or chronic viral infection and susceptibility to disease. Of particular interest are the 60 non-*HLA* coding genes within the MHC class III region, many of which have a role in regulating inflammation or have strong associations with susceptibility to diseases, such as rheumatoid arthritis (14), myocardial infarction (15), malaria (16), septic shock (17), and Ehlers – Danlos syndrome (18). The statistical analysis of extensive linkage disequilibrium (LD) across the entire 3.6-Mb MHC region has resulted in the detection and categorization of population-specific HLA haplotypes based on the allelic distribution and allelic combination of different MHC genes (19–21).

Although HCV appears to infect humans regardless of their *HLA* genotypes, the classical *HLA* alleles may determine the natural history of the viral infection in the post-infectious stage, such as viral resolution, the progression/suppression of persistent infection, and liver disease. For example, *HLA-B*44-DRB1*1302-DQB1*0604* haplotype carriers remain asymptomatic, whereas *B*54-DRB1*0405-DQB1*0401* carriers tend to develop chronic liver disease (22). Therefore, we hypothesized that either particular *HLA* or non-*HLA* gene alleles might regulate the development of DCM and/or HCM after HCV infection. In this study, we undertook genotyping to map the HLA-linked susceptibility loci for HCV-DCM and HCV-HCM in order to better understand the immuno-genetic factors controlling the clinical outcome of chronic HCV infection. This is the first genetic study to demonstrate that a non-*HLA* locus within the MHC class III – class I boundary region may confer the susceptibility to HCV-DCM in Japanese.

Materials and methods

Subjects

Diagnosis of DCM and HCM was based on the criteria of the Japan Research Committee on Idiopathic Cardiomyopathy developed with guidance from the report by the 1980 World Health Organization/International Society and Federation of Cardiology task force on the definition and classification of cardiomyopathies (23, 24). Among the Japanese patients who conformed with the diagnostic criteria, a total of 59 patients positive for the anti-HCV antibody (21 patients of HCV-DCM and 38 patients of HCV-HCM) were enrolled in this study along with 120 healthy controls after obtaining informed consent. All of them were genetically unrelated. Genomic DNAs were extracted by the guanidine hydrochloride method from each peripheral blood sample. The study protocol was approved by the Ethics Reviewing Committee of Tokai University School of Medicine.

Genotyping for microsatellite polymorphisms

Genotyping was performed with 19 microsatellite markers located within the MHC genomic region to identify the susceptibility locus for HCV-DCM and/or HCV-HCM. The marker order, genomic distances, and primer sequence were described previously (25, 26). Each forward primer was synthesized by labeling at the 5′ end with a fluorochrome 6-FAM, HEX, or TET (Applied Biosystems, Foster City, CA, USA). The fragment samples were mixed with formamide-containing stop buffer and GeneScan-500 ROX size standard (Applied Biosystems) and separated by GeneScan system on a 377 DNA sequencer (Applied Biosystems). Repeat fragment sizes were assigned by GENOTYPER software (Applied Biosystems).

Genotyping for two classical *HLA* genes, *HLA-B*, and *HLA-Cw*

The high resolution typing for *HLA-B* and *HLA-Cw* was performed by the sequence-based typing (SBT) method according to standard procedures (Forensic Analytical, Hayward, CA, USA). The MATCHMAKER allele Identification program (Applied Biosystems) was used to assign the *HLA* alleles.

Genotyping for five non-*HLA* genes, *TNF*, *LTA*, *NFKBIL1*, *ATP6V1G2*, and *BAT1*

A total of 23 single nucleotide polymorphisms (SNPs) as shown in Fig. 2 were examined in this study. The tumor necrosis factor (*TNF*), nuclear factor of kappa light polypeptide gene enhancer in B-cells inhibitor-like 1 also known as *IkBL* (*NFKBIL1*), and HLA-B associated transcript 1 (*BAT1*) genes were genotyped by the direct sequencing method using the primer sets as previously reported

Primers used for genotyping the candidate genes, *LTA* and *ATP6V1G2*

Gene	Target	Name	Primer sequence (5′–3′)	Length (mer)	Product (bp)	Annealing (°C)
LTA						
	+80C/A	LTA1F2	CTC CAC ACA GCA GGT GAG G	19	172	58
		LTA1R2	CCA AAA CCA AAC CCA CCA AG	20		
	+252A/G	LTA1F	GCT TCG TGC TTT GGA CTA CC	20	714	60
		LTA3R	GGG AGG TCA GGT GGA TGT TTA C	22		
ATP6V1G2 (ATP6G)						
	Exon1	ATPex1F	AGG AGG ACC AGT CAT CAA TAG GAG	24	306	66
		ATPex1R	CTA AGG GAG GAA AGA GGA GAC TCA	24		
	Exon2 and *+760A/T* (rs2523502)	ATPex2F	GGG ACT GAC TCC TGC TAT TAC ATT G	25	247	64
		ATPex2R	CAC CCT TAC ACA CCT CAC TAG ATG C	25		
	Exon3 and *+1222C/T* (rs2239705)	ATPex3F	CTT TCT TCT AGG CTT TGT TTC AGG A	25	527	62
		ATPex3R	CAA ATT TCA CAG AGG GTT TAG GTG A	25		

Table 1

(27–29). The *ATP6V1G2* gene was analyzed for all exons in addition to two intronic SNPs, *ATP6V1G2*+760* (dbSNP accession number rs2523502) and *ATP6V1G2*+1222* (rs2239705), through the direct sequencing method by primer sets as listed in Table 1. Cycle sequencing was performed using the Big-Dye Terminator system (Applied Biosystems). The sequencing analysis was conducted with an ABI Prism 377 DNA sequencer (Applied Biosystems). The genotypes were determined by manual comparison of patients' sequences with a public reference sequence (GeneBank accession number AB063177). In the *LTA* (lymphotoxin-alpha) gene, alleles carried at +80 and +252 (30) were screened by the PCR-single strand conformation polymorphism analysis and the PCR-restriction fragment length polymorphism method at the *Nco* I site, respectively.

Statistical analysis

The Hardy – Weinberg equilibrium distribution for the SNPs and their haplotypes was assessed by Fisher's exact test with Bonferroni's inequality method. The statistical significance was assigned at P and corrected P (Pc) values of less than 0.05. The strength of the association with HCV-DCM and/or HCV-HCM was evaluated by odds ratio (OR) with 95% confidence interval. The R package 'haplo.stats' (http://www.r-project.org/) was used to evaluate haplotype structure carrying the disease-associated markers around the candidate region. On the basis of the haplotype structure, the LD around the candidate region was measured in both patients and controls with two LD coefficients, Lewontin's D' and Hill's r^2, obtained from the R package 'genetics' (http://www.r-project.org/).

Results

Susceptibility gene mapping for HCV-associated cardiomyopathy with microsatellite markers encompassing the MHC genomic region

In an initial association analysis, we carried out a region-wide scan using 19 microsatellite markers dispersed throughout the MHC region. The multipoint analysis displayed different association profiles between HCV-DCM and HCV-HCM as illustrated in Fig. 1. In the analysis of HCV-DCM, significant associations were observed with two markers positioned around the boundary region between class III and class I: *STR-MICA*183* (OR = 4.59, $P = 0.005$, $Pc = 0.026$) and *C1-4-1*225* (OR = 3.57, $P = 0.006$, $Pc = 0.042$). Because LD of microsatellite markers usually extend some hundred kb, we considered a approximately 300-kb interval as a potential susceptibility locus for HCV-DCM, which contains 9 genes as follows; *TNF*, *LTA*, *NFKBIL1*, *ATP6V1G2* (vacuolar ATP synthase subunit G 2; also known as *ATP6G*), *BAT1*, *MICB* (MHC class I′ chain-related protein B), *MICA* (MHC class I chain-related gene A protein), *HLA-B*, and *HLA-Cw* (Fig. 2). In clear contrast, there were no significant associations between the HCV-HCM and the microsatellite markers in the MHC region.

Screening of SNP in association with the susceptibility to HCV-DCM in seven candidate genes

To identify the susceptibility gene, we examined SNPs in each of the candidate genes and compared their individual as well as their combined (haplotype) frequencies between the HCV-DCM patients and control individuals (Table 2). Of 16 *HLA-B* and 9 *HLA-Cw* alleles assigned by SBT method in HCV-DCM patients, *HLA-B*0702* (OR = 3.96, $P = 0.022$, $Pc = 0.356$) and *HLA-Cw*0702* (OR = 3.00, $P = 0.019$, $Pc = 0.192$) showed marginally significant associations with HCV-DCM. Additionally, of the seven non-*HLA* genes, we analyzed five genes, *TNF*, *LTA*, *NFKBIL1*, *ATP6V1G2*, and *BAT1*, in the SNP study and found three SNPs strongly associated with HCV-DCM; a T insertion at the position −421 of the *NFKBIL1* promoter (*NFKBIL1p*−421insT*) (OR = 4.25, $P = 0.003$, $Pc = 0.006$), an A to T substitution at the position +760 of the *ATP6V1G2* (*ATP6V1G2*+760T*) (OR = 4.25, $P = 0.003$, $Pc = 0.006$), and a fifth polymorphic haplotype (*BAT1p*05*) of the *BAT1* promoter (OR = 4.25, $P = 0.003$, $Pc = 0.006$) (Table 2). The *NFKBIL1p*−421insT* and *ATP6V1G2*+760T* are characteristic polymorphisms of the *NFKBIL1p*02* and *ATP6V1G2*3* alleles, respectively, which exhibited equivalent associations with HCV-DCM (Table 2). In contrast, neither *TNF* nor *LTA* polymorphisms showed significant association with HCV-DCM (data not shown).

Pairwise LD mapping around the candidate region in the Japanese population

Interestingly, the combination of the non-*HLA* gene alleles, consisting of *NFKBIL1p*02*, *ATP6V1G2*3*, and *BAT1p*05*, which were

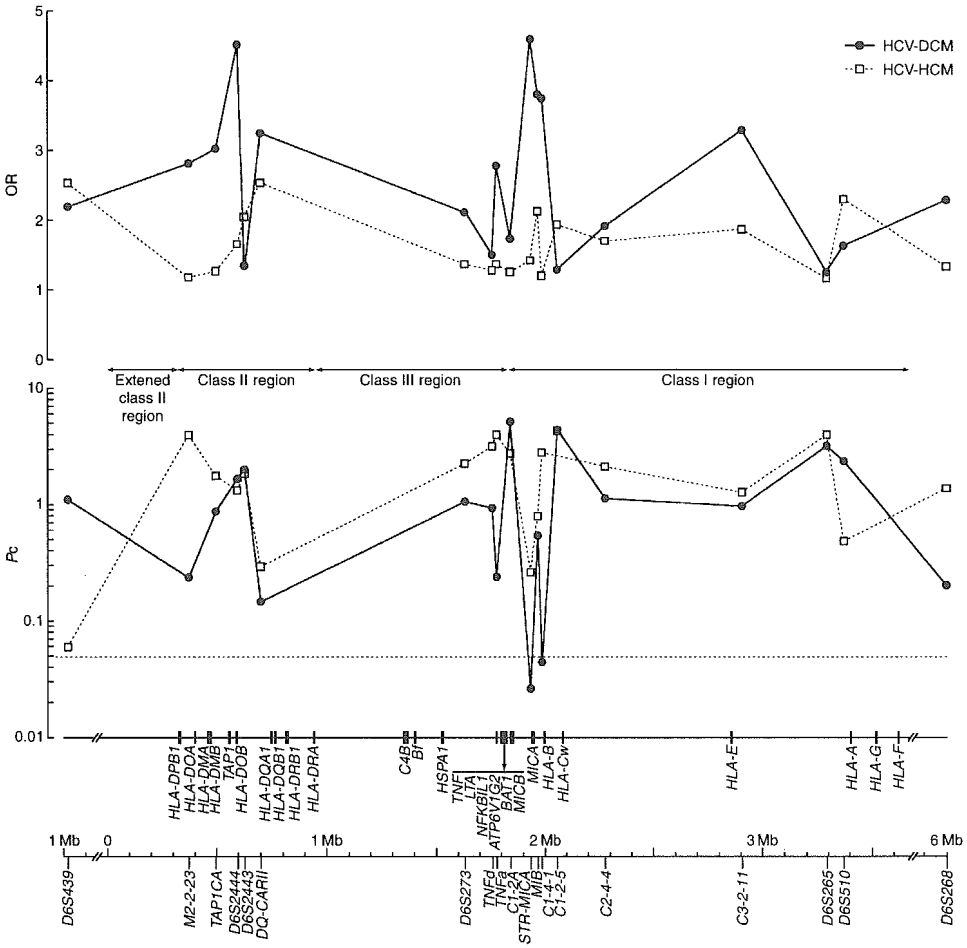

Fig. 1. **The susceptibility gene mapping for hepatitis C virus-associated dilated cardiomyopathy (HCV-DCM) and HCV-hypertrophic cardiomyopathy (HCV-HCM) with microsatellite markers throughout the human major histocompatibility complex genomic region.** Corrected *P* (*Pc*) value with logarithmic scale and odds ratio (*y*-axis) were plotted against physical location of the microsatellite markers on chromosome 6p21.3 (*x*-axis), their distance (in kb) in order from centromere to telomere. The dotted horizontal line shows the threshold for 5% significance after correcting for multiple testing.

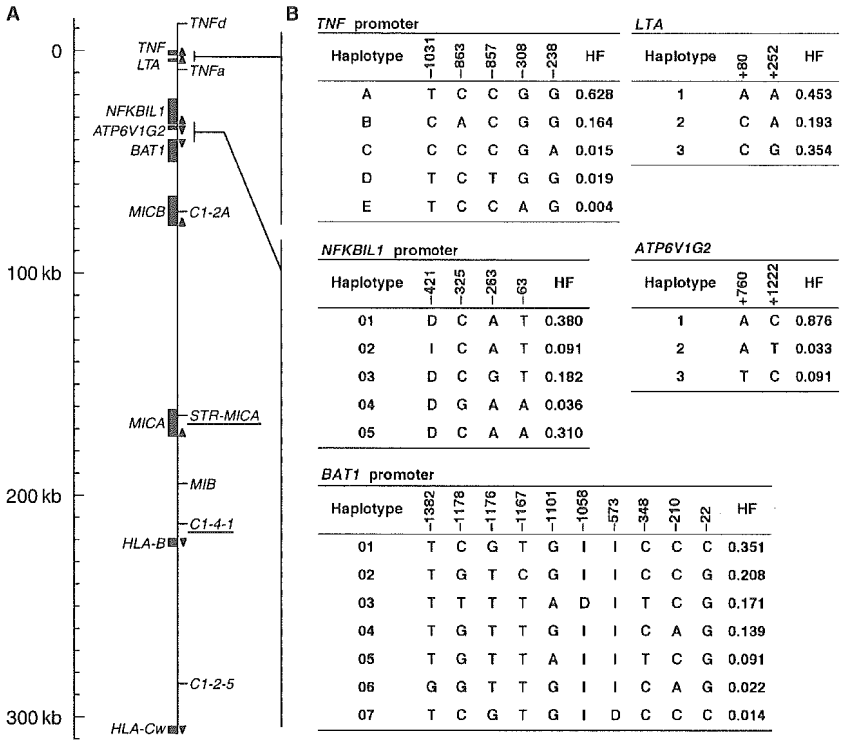

TNF promoter

Haplotype	−1031	−863	−857	−308	−238	HF
A	T	C	C	G	G	0.628
B	C	A	C	G	G	0.164
C	C	C	C	G	A	0.015
D	T	C	T	G	G	0.019
E	T	C	C	A	G	0.004

LTA

Haplotype	+80	+252	HF
1	A	A	0.453
2	C	A	0.193
3	C	G	0.354

NFKBIL1 promoter

Haplotype	−421	−325	−263	−63	HF
01	D	C	A	T	0.380
02	I	C	A	T	0.091
03	D	C	G	T	0.182
04	D	G	A	A	0.036
05	D	C	A	A	0.310

ATP6V1G2

Haplotype	+760	+1222	HF
1	A	C	0.876
2	A	T	0.033
3	T	C	0.091

BAT1 promoter

Haplotype	−1382	−1178	−1176	−1167	−1101	−1058	−573	−348	−210	−22	HF
01	T	C	G	T	G	I	I	C	C	C	0.351
02	T	G	T	C	G	I	I	C	C	G	0.208
03	T	T	T	T	A	D	I	T	C	G	0.171
04	T	G	T	T	G	I	I	C	A	G	0.139
05	T	G	T	T	A	I	I	T	C	G	0.091
06	G	G	T	T	G	I	I	C	A	G	0.022
07	T	C	G	T	G	I	D	C	C	C	0.014

Fig. 2. **Candidate gene mapping in a susceptible 300-kb interval to hepatitis C virus-associated dilated cardiomyopathy (HCV-DCM).** (A) The physical map of candidate genes and genetic markers in the 300-kb interval. Microsatellite markers showing strong association with HCV-DCM in the microsatellite analyses were underlined. Arrow heads indicated the transcriptional direction of candidate genes. (B) Haplotype structures at the candidate gene loci. Haplotype frequencies (HF) were estimated by EM algorithms in the R package 'haplo.stats' (http://www.r-project.org/). Designations refer to the nucleotide position to transcriptional start site. Allelic sequences were defined by the same forward sequence as transcriptional direction in the genes. The I and D carried at *NFKBIL1p*−421*, *BAT1p*−1058*, and *BAT1p*−573* indicate the insertion and the deletion (indel), respectively. The indels carry allelic forms as follows (in order from 5′ to 3′): T/− at the *NFKBIL1p*−421*, AGG/− at the *BAT1p*−1058*, and CATCAGCTACCTCGGA/− at the *BAT1p*−573*.

significantly associated with HCV-DCM were tightly linked as a non-HLA haplotype block in a one-to-one correspondence in both patients and controls. This linkage was expected to result from a characteristic LD relationship in Japanese. We, therefore, evaluated the LD indexes for the specific LD block using other 15 polymorphic markers around the central MHC genomic region in the Japanese controls (Table 3). The pairwise LD mapping confirmed that these three alleles are in complete LD with each other, showing LD index being 1.0 for D' and 1.0 for r^2. In addition, *HLA-B*0702* was in strong LD not only with *HLA-Cw*0702* ($D' = 1.0$, $r^2 = 0.43$) but also with this non-HLA haplotype block ($D' = 1.0$, $r^2 = 0.59$).

The risk evaluation of the patient-shared block in HCV-DCM

We subsequently evaluated the non-HLA haplotype block as the main risk marker for HCV-DCM (Table 4). The analysis showed that a higher risk was conferred by *Hap A* (OR = 6.75, $P = 0.0003$, $Pc = 0.0081$) from the MHC class III − class I boundary region than by *Hap B* (OR = 3.96, $P = 0.02$, $Pc = 0.40$) from the MHC class I region. This strongly suggests that the disease susceptibility to HCV-DCM is controlled mainly by the non-*HLA* genes in the MHC class III − class I boundary region rather than by the classical *HLA* class I genes. The strong LD between *TNF* gene cluster and *NFKBIL1-BAT1* block also prompted us to examine a synergistic risk for HCV-DCM between *TNFp*A-LTA*1* and *NFKBIL1p*02-ATP6V1G2*3-BAT1*05-C1-2A*242-STR-MICA*183* by two-locus-analysis method of Svejgaard and Ryder (31). However, no synergistic risk between the haplotypes was found (data not shown). In light of location of the polymorphic markers composing of *Hap A*, the primary susceptibility locus could be narrowed down to approximately 133-kb interval between the *NFKBIL1* and *MICA* genes.

Discussion

It is well established that the *HLA* genes in the MHC have an important role in the regulation of immune response to acute and persistent HCV infection. The aim of this study was to investigate whether the non-*HLA* genes and *HLA* genes in the MHC might be associated with the susceptibility to HCV-DCM and/or HCV-HCM. Our MHC region-wide association study mapped the HCV-DCM susceptibility locus to the region spanning from *NFKBIL1* to *MICA* within the MHC class III − class I boundary region. In addition, the polymorphisms located around this boundary region were in LD with the classical *HLA-B* and *HLA-Cw* class I gene alleles. These observations suggest that the susceptibility to HCV-DCM may

Associations of candidate gene polymorphisms relevant to hepatitis C virus-associated dilated cardiomyopathy susceptibility within the central major histocompatibility complex region

	Genotype[a]									
	Cases (n = 21)			Controls (n = 120)			Carriers versus non-carriers			
Marker	++	+−	−−	++	+−	−−	OR	95% CI	*P*	*Pc*
Allele										
*NFKBIL1p*02*	1	8	12	0	18	102	4.25	1.57 - 11.54	0.003	0.014
*ATP6V1G2*3*	1	8	12	0	18	102	4.25	1.57 - 11.54	0.003	0.008
*BAT1p*05*	1	8	12	0	18	102	4.25	1.57 - 11.54	0.003	0.014
*HLA-B*0702*	0	6	15	0	11	109	3.96	1.28 - 12.29	0.022	0.356
*HLA-Cw*0702*	1	8	12	0	24	96	3.00	1.13 - 7.94	0.019	0.192
Polymorphism										
−421insT of NFKBIL1	1	8	12	0	18	102	4.25	1.57 - 11.54	0.003	0.005
+760T of ATP6V1G2	1	8	12	0	18	102	4.25	1.57 - 11.54	0.003	0.005

[a]++, homozygous carrier with the targeted polymorphisms; +−, heterozygous; −−, non-carrier

Table 2

be controlled by the non-*HLA* genes in LD with the *HLA* class I gene alleles rather than the *HLA* genes.

The mapped candidate susceptibility gene locus for HCV-DCM within the MHC class III – class I boundary region overlaps the susceptibility/resistance loci for some autoimmune diseases, such as rheumatoid arthritis (14) and insulin-dependent diabetes mellitus (32). Some candidate genes within the class III – class I boundary region that control the susceptibility to HCV-DCM encode molecules that are probably involved in immunity and inflammation. For example, *NFKBIL1* gene encodes a I-kappa-B-like molecule (33), which localizes within nuclear speckles (34). The product of *ATP6V1G2* gene responds to IL-1 as a subunit of vacuolar ATPase H^+ pump and modulates macrophage effector functions (35, 36). The role of the BAT1 proteins is less well defined, but they may act as negative regulators of an inflammatory cytokine (37) and effect cell proliferation in various human tissues including the heart (38). *MICA* and *MICB* genes exhibit a restricted expression pattern on cell in stress like those after viral infection (39–41) and may play a role in HCV infectious status as ligand of NKG2D (42, 43). These reported functions for the five non-*HLA* genes around the MHC class III – class I boundary region are helpful in explaining the genetic background of HCV-DCM, but cellular studies are clearly needed to determine the direct effect of HCV infection on the activity and the role of *NFKBIL1*, *ATP6V1G2*, *BAT1*, *MICB*, and *MICA* genes in the heart.

The candidate susceptibility locus identified in this study contained several functional SNPs, which might regulate transcriptional efficiency of the candidate genes. One such interesting SNPs is *NFKBIL1p*−62T/A* that lies within an E-box-binding motif (CANNTG) for transcriptional factors, E47 and USF1 (44). Second, the sequence spanning *BAT1p*−22G/C* (GCAGAT) and *BAT1p*−348C/T* (CCAT) is known to affect the *BAT1* expression via direct interaction with their transcriptional factors, Oct1 and YY1, respectively (45). These multiple functional polymorphisms may therefore combine functionally to increase the risk of DCM under the HCV infection. There were, however, still many ethnically characteristic and/or functionally unknown promoter polymorphisms other than the aforementioned SNPs. A transgenic mouse study revealed that the HCV-core protein is directly involved in the development of cardiomyopathy (46). The extent to which such polymorphisms influence the pathogenesis of HCV-DCM is a subject of further study.

Despite the same viral etiology, HCV involvement in cardiomyopathy can result in two distinct clinical outcomes, HCV-DCM and HCV-HCM, and a difference in the association with the MHC was revealed in this study. Whereas the microsatellite markers displayed a significant association of a particular MHC subregion with HCV-DCM, there was no significant association between the MHC and HCV-HCM. The HLA haplotypic markers in association with HCV-DCM are in strong LD with *B*0702-Cw*0702*, which are in LD with *DRB1*0101-DQB1*0501* in Japanese (47). However, these *HLA* alleles were not associated with HCV-associated liver diseases (22). In addition, a tendency toward severe HCV-infection status in Spanish whites was associated with *HLA-DR3-MICA-A4-HLA-B*18* (48); however, HCV-DCM patients in the present study showed

Pairwise linkage disequilibrium (LD) analysis of hepatitis C virus-associated dilated cardiomyopathy susceptibility loci for 120 Japanese individuals

		r^2														
Locus		*TNFd*130*	*TNFp*A*	*LTA*1*	*TNFa*115*	*NFKBIL1p*02*	*ATP6V1G2*3*	*BAT1p*05*	*C1-2A*242*	*STR-MICA*183*	*MIB*336*	*C1-4–1*225*	*HLA-B*0702*	*C1-2-5*200*	*HLA-Cw* 0702*	*C2-4-4* 231*
	*TNFd*130*	–	0.19	0.23	0.30	0.14	0.14	0.14	0.52	0.01	0.04	0.07	0.09	0.01	0.06	0.03
	*TNFp*A*	0.46	–	0.00	0.04	0.05	0.05	0.05	0.15	0.01	0.06	0.01	0.03	0.04	0.00	0.01
	*LTA*1*	0.59	0.06	–	0.16	0.10	0.10	0.10	0.31	0.01	0.01	0.05	0.06	0.01	0.05	0.01
	*TNFa*115*	**0.95**	0.35	**0.85**	–	0.32	0.32	0.32	0.35	0.05	0.13	0.08	0.25	0.04	0.12	0.06
	*NFKBIL1p*02*	**1.00**	**1.00**	**1.00**	**0.86**	–	**1.00**	**1.00**	0.16	0.24	0.26	0.34	**0.59**	0.14	0.33	0.05
	*ATP6V1G2*3*	**1.00**	**1.00**	**1.00**	**0.86**	**1.00**	–	**1.00**	0.16	0.24	0.26	0.34	**0.59**	0.14	0.33	0.05
	*BAT1p*05*	**1.00**	**1.00**	**1.00**	**0.86**	**1.00**	**1.00**	–	0.16	0.24	0.26	0.34	**0.59**	0.14	0.33	0.05
D'	*C1-2A*242*	**0.85**	0.47	0.80	**0.87**	**0.90**	**0.90**	**0.90**	–	0.04	0.04	0.07	0.12	0.04	0.06	0.03
	*STR-MICA*183*	0.23	0.35	0.20	0.26	0.66	0.66	0.66	0.34	–	0.18	0.16	0.32	0.04	0.14	0.09
	*MIB*336*	0.46	**1.00**	0.26	0.50	0.55	0.55	0.55	0.39	0.53	–	0.34	**0.50**	0.10	0.21	0.01
	*C1-4-1*225*	0.66	0.45	0.69	0.40	0.62	0.62	0.62	0.54	0.50	0.60	–	**0.53**	0.08	**0.64**	0.06
	*HLA-B*0702*	**1.00**	**1.00**	**1.00**	**1.00**	**1.00**	**1.00**	**1.00**	**1.00**	**1.00**	**1.00**	**1.00**	–	0.23	**0.43**	0.05
	*C1-2-5*200*	0.18	0.55	0.16	0.21	0.61	0.61	0.61	0.28	0.25	0.46	0.43	**1.00**	–	0.06	0.12
	*HLA-Cw*0702*	0.55	0.10	0.61	0.46	0.67	0.67	0.67	0.46	0.44	0.49	**0.89**	**1.00**	0.34	–	0.11
	*C2-4-4*231*	0.22	0.11	0.08	0.57	0.79	0.79	0.79	0.30	0.79	0.40	**0.81**	**1.00**	0.77	**1.00**	–

Each polymorphic marker was positioned in order from major histocompatibility complex class III to class I subregion. The degree of LD is shown as the LD index of Lewontin correlation (D') in the lower left triangle and Pearson correlation (r^2) in the upper right triangle. Bold number indicates the strong LD: $D' > 0.8$, $r^2 > 0.4$. The solid LD block of genes from the class III region with the highest LD are boxed.

Table 3

Haplotype structures composed of significantly increased markers and single nucleotide polymorphisms (SNPs) in HCV-associated dilated cardiomyopathy

	Diplotype[a]									
	Cases (n = 21)			Control (n = 120)			Carriers versus non-carriers			
Haplotype	++	+−	−−	++	+−	−−	OR	95% CI	P	P_C
Hap A (MHC class III – class I boundary region side)										
*NFKBIL1p*02-ATP6V1G2*3-BAT1p*05-STR-MICA*183*	1	8	12	0	13	107	6.17	2.19 – 17.45	0.0005	0.0131
Hap B (MHC class I region)										
*B*0702-Cw*0702*	0	6	15	0	11	109	3.96	1.28 – 12.29	0.02	0.40

[a]++, homozygous carrier with the targeted haplotypes; +−, heterozygous; −−, non-carrier

Table 4

a different association with the *DRB1*0101-STR-MICA*183* (also known as *MICA-A5.1)-B*0702* haplotype. These haplotypic differences may indirectly reflect the genetic diversity among non-*HLA* genes that define each HLA haplotypes. Thus, these observations support the view that distinct genetic factors can affect the clinical outcome by regulating pathogenic pathway after the viral infection.

In summary, our susceptibility gene mapping showed that the non-*HLA* gene block consisting of the *NFKBIL*, *ATP6V1G2*, *BAT1*, *MICB*, and *MICA* genes within the MHC class III – class I boundary region was strongly associated with the susceptibility to HCV-DCM, whereas there was no significant association between the MHC genomic region and HCV-HCM. Through the disparity in the disease-associated HLA markers, we hypothesize that HCV-DCM and HCV-HCM have at least two distinct pathogenic mechanisms in relation to the MHC-meditated immune response, although the patients that developed DCM/HCM with HCV infection consisted of a small number of cases. Because the conclusions were based on the analysis of small number of patients, other independent studies with larger number of patients will be required. Nevertheless, our findings may provide an important clue as to the underlying cause of HCV-DCM in terms of immunogenetics. Because of tight LD among non-*HLA* alleles within the candidate genes, we could not identify specific susceptibility gene for HCV-DCM. Therefore, analysis of central MHC region in other Asian ethnic groups with HCV-DCM may contribute to a delineation of primary locus to the HCV-DCM susceptibility. Genome-wide microsatellite association studies in a much larger sample of infected patients will be also required to comprehensively understand their genetic background and the effect of genetic diversity on the outcome of HCV-associated cardiomyopathies.

References

1. Higuchi M, Tanaka E, Kiyosawa K. Epidemiology and clinical aspects on hepatitis C. *Jpn J Infect Dis* 2002: **55**: 69–77.
2. Mayo MJ. Extrahepatic manifestations of hepatitis C infection. *Am J Med Sci* 2003: **325**: 135–48.
3. Yan FM, Chen AS, Hao F et al. Hepatitis C virus may infect extrahepatic tissues in patients with hepatitis C. *World J Gastroenterol* 2000: **6**: 805–11.
4. Matsumori A, Matoba Y, Sasayama S. Dilated cardiomyopathy associated with hepatitis C virus infection. *Circulation* 1995: **92**: 2519–25.
5. Matsumori A, Matoba Y, Nishio R et al. Detection of hepatitis C virus RNA from the heart of patients with hypertrophic cardiomyopathy. *Biochem Biophys Res Commun* 1996: **222**: 678–82.
6. Takeda A, Sakata A, Takeda N. Detection of hepatitis C virus RNA in the hearts of patients with hepatogenic cardiomyopathy. *Mol Cell Biochem* 1999: **195**: 257–61.
7. Teragaki M, Nishiguchi S, Takeuchi K et al. Prevalence of hepatitis C virus infection among patients with hypertrophic cardiomyopathy. *Heart Vessels* 2003: **18**: 167–70.
8. Matsumori A, Ohashi N, Hasegawa K et al. Hepatitis C virus infection and heart diseases: a multicenter study in Japan. *Jpn Circ J* 1998: **62**: 389–91.
9. Cooke GS, Hill AV. Genetics of susceptibility to human infectious disease. *Nat Rev Genet* 2001: **2**: 967–77.
10. Shiina T, Inoko H, Kulski JK. An update of the HLA genomic region, locus information and disease associations: 2004. *Tissue Antigens* 2004: **64**: 631–49.
11. Marsh SG, Albert ED, Bodmer WF et al. Nomenclature for factors of the HLA system, 2002. *Hum Immunol* 2002: **63**: 1213–68.
12. Robinson J, Waller MJ, Parham P et al. IMGT/HLA and IMGT/MHC: sequence databases for the study of the major histocompatibility complex. *Nucl Acids Res* 2003: **31**: 311–4.
13. Mungall AJ, Palmer SA, Sims SK et al. The DNA sequence and analysis of human chromosome 6. *Nature* 2003: **425**: 805–11.

14. Okamoto K, Makino S, Yoshikawa Y et al. Identification of I kappa BL as the second major histocompatibility complex-linked susceptibility locus for rheumatoid arthritis. *Am J Hum Genet* 2003: **72**: 303–12.
15. Ozaki K, Ohnishi Y, Iida A et al. Functional SNPs in the lymphotoxin-alpha gene that associated with susceptibility to myocardial infraction. *Nat Genet* 2002: **32**: 650–4.
16. Knight JC, Udalova I, Hill AV et al. A polymorphism that affects OCT-1 binding to the TNF promoter region is associated with severe malaria. *Nat Genet* 1999: **22**: 145–50.
17. Mira J. Association of TNF2, a TNF-alpha promoter polymorphism, with septic shock susceptibility and mortality: a multicenter study. *JAMA* 1999: **282**: 561–8.
18. Burch GH, Gong Y, Liu W et al. Tenascin-X deficiency is associated with Ehlers-Danos syndrome. *Nat Genet* 1997: **17**: 104–8.
19. Ahmad T, Neville M, Marshall SE et al. Haplotype-specific linkage disequilibrium patterns define the genetic topography of the human MHC. *Hum Mol Genet* 2003: **12**: 647–56.
20. Walsh EC, Mather KA, Schaffner SF et al. An integrated haplotype map of the human major histocompatibility complex. *Am J Hum Genet* 2003: **73**: 580–90.
21. Stenzel A, Lu T, Koch WA et al. Patterns of linkage disequilibrium in the MHC region on human chromosome 6p. *Hum Genet* 2004: **114**: 377–85.
22. Kuzushita N, Hayashi N, Moribe T et al. Influence of HLA haplotypes on the clinical courses of individuals infected with hepatitis C virus. *Hepatology* 1998: **27**: 240–4.
23. Research Committee on Idiopathic Cardiomyopathy, the Ministry of the Health and Welfare, Japan. Guidelines for the diagnosis of idiopathic cardiomyopathy. In: *Annual Report of the Research Committee on Idiopathic Cardiomyopathy, the Ministry of the Health and Welfare, Japan*, 1985: 13–5 (in Japanese).
24. The WHO, /ISFC task force on the definition and classification of cardiomyopathies. Report of the WHO/ISFC task force on the definition and classification of cardiomyopathies. *Br Heart J* 1980: **44**: 672–3.
25. Foissac A, Salhi M, Cambon-Thomsen A. Microsatellites in the HLA region: 1999 update. *Tissue Antigens* 2000: **55**: 477–509.
26. Cullen M, Malasky M, Harding A, Carrington M. High-density map of short tandem repeats across the human major histocompatibility complex. *Immunogenetics* 2003: **54**: 900–10.
27. Higuchi T, Seki N, Kamizono S et al. Polymorphism of the 5′-flanking region of the human tumor necrosis factor (TNF)-alpha gene in Japanese. *Tissue Antigens* 1998: **51**: 605–12.
28. Allcock RJ, Baluchova K, Cheong KY, Price P. Haplotypic single nucleotide polymorphisms in the central MHC gene IKBL, a potential regulator of NF-kappaB function. *Immunogenetics* 2001: **52**: 289–93.
29. Wong AM, Allcock RJ, Cheong KY, Christiansen FT, Price P. Alleles of the proximal promoter of BAT1, a putative anti-inflammatory gene adjacent to the TNF cluster, reduce transcription on a disease-associated MHC haplotype. *Genes Cells* 2003: **8**: 403–12.
30. Knight JC, Keating BJ, Kwiatkowski DP. Allele-specific repression of lymphotoxin-alpha by activated B cell factor-1. *Nat Genet* 2004: **36**: 394–9.
31. Svejgaard A, Ryder LP. HLA and disease associations: detecting the strongest association. *Tissue Antigens* 1994: **43**: 18–27.
32. Yamashita T, Hamaguchi K, Kusuda Y . IKBL promoter polymorphism is strongly associated with resistance to type 1 diabetes in Japanese. *Tissue Antigens* 2004: **63**: 223–30.
33. Albertella MR, Campbell RD. Characterization of a novel gene in the human major histocompatibility complex that encodes a potential new member of the I kappa B family of proteins. *Hum Mol Genet* 1994: **3**: 793–9.
34. Semple JI, Brown SE, Sanderson CM et al. A distinct bipartite motif is required for the localization of inhibitatory kappaB-like (IkappaBL) protein to nuclear speckles. *Biochem J* 2002: **361**: 489–96.
35. Conboy IM, Manoli D, Mhaiskar V, Jones PP. Calcineurin and vacuolar-type H+-ATPase modulate macrophage effector functions. *Proc Natl Acad Sci USA* 1999: **96**: 6324–9.
36. Brisseau GF, Grinstein S, Hackam DJ et al. Interleukin-1 increases vacuolar-type H+-ATPase activity in murine peritoneal macrophages. *J Biol Chem* 1996: **27**: 2005–11.
37. Allcock RJ, Williams JH, Price P. The central MHC gene, BAT1, may encode a protein that down-regulates cytokine production. *Genes Cells* 2001: **6**: 487–94.
38. Leaw CL, Ren EC, Choong ML. Hcc-1 is a novel component of the nuclear matrix with growth inhibitory function. *Cell Mol Life Sci* 2004: **61**: 2264–73.
39. Groh V, Bahram S, Bauer S et al. Cell stress-regulated human major histocompatibility complex class I gene expressed in gastrointestinal epithelium. *Proc Natl Acad Sci USA* 1996: **93**: 12445–50.
40. Zwirner NW, Dole K, Stastny P. Differential surface expression of MICA by endothelial cells, fibroblasts, keratinocytes, and monocytes. *Hum Immunol* 1999: **60**: 323–30.
41. Molinero LL, Fuertes MB, Girart MV et al. NF-kappa B regulates expression of the MHC class I-related chain A gene in activated T lymphocytes. *J Immunol* 2004: **173**: 5583–90.
42. Karacki PS, Gao X, Thio CL et al. MICA and recovery from hepatitis C virus and hepatitis B virus infections. *Genes Immun* 2004: **5**: 261–6.
43. Jinushi M, Takehara T, Tatsumi T et al. Autocrine/paracrine IL-15 that is required for type I IFN-meditated dendritic cell expression of MHC class I-related chain A and B is impaired in hepatitis C virus infection. *J Immunol* 2003: **171**: 5423–9.
44. Boodhoo A, Wong AM, Williamson D et al. A promoter polymorphism in the central MHC gene, IKBL, influences the binding of transcription factors USF1 and E47 on disease-associated haplotypes. *Gene Exp* 2004: **12**: 1–11.
45. Price P, Wong AM, Williamson D et al. Polymorphisms at positions -22 and – 348 in the promoter of the BAT1 gene affect transcription and the binding of nuclear factors. *Hum Mol Genet* 2004: **13**: 967–74.
46. Omura T, Yoshiyama M, Hayashi T et al. Core protein hepatitis C virus induces cardiomyopathy *Circ Res* 2005: **96**: 148–50.
47. Saito S, Ota S, Yamada E, Inoko H, Ota M. Allele frequencies and haplotypic associations defined by allelic DNA typing at HLA class I and class II loci in the Japanese population. *Tissue Antigens* 2000: **56**: 522–9.
48. López-Vázquez A, Rodrigo L, Miña-Blanco A et al. Extended human leukocyte antigen haplotype EH18.1 influences progression to hepatocellular carcinoma in patients with hepatitis C virus infection. *J Infect Dis* 2004: **189**: 957–63.

ARTICLE IN PRESS

Available online at www.sciencedirect.com
SCIENCE DIRECT®

ELSEVIER

Biochemical and Biophysical Research Communications 341 (2006) 573–582

BBRC

www.elsevier.com/locate/ybbrc

Bioengineered cardiac cell sheet grafts have intrinsic angiogenic potential

Sachiko Sekiya, Tatsuya Shimizu, Masayuki Yamato, Akihiko Kikuchi, Teruo Okano *

Institute of Advanced Biomedical Engineering and Science, Tokyo Women's Medical University, 8-1 Kawada-cho, Shinjuku-ku, Tokyo 162-8666, Japan

Received 16 December 2005

Abstract

Previously, we have demonstrated the long-term survival of myocardial cell sheet constructs in vivo, with microvascular network formation throughout the engineered tissues. The understanding and control of these vascularization processes are a key factor for creating thicker functional tissues. Here, we show that cardiac cell sheets express angiogenesis-related genes and form endothelial cell networks in culture. After non-invasive harvest and stacking of cell sheets using temperature-responsive culture dishes, these endothelial cell networks are maintained and result in neovascularization upon in vivo transplantation. Interestingly, we also discovered that all of the graft vessels are derived from the grafts themselves and these vessels migrate to connect with the host vasculature. Finally, blood vessel formation within the grafts can be controlled by changing the ratio of endothelial cells. In conclusion, myocardial tissue grafts engineered with cell sheet technology have their own inherent potential for the in vivo neovascularization that can be regulated in vitro.

Keywords: Angiogenesis; Vascularization; Myocardial tissue graft; Tissue engineering; Cell sheet

Blood capillaries are precisely organized throughout nearly all tissues and support normal organ function via the supply of nutrients, as well as the removal of various metabolic wastes. In particular, the heart with its high metabolic activity has an increased need for nutrient supplementation and thus possesses an abundant vascular network. Capillary formation within these tissues occurs via two basic vessel-constructing processes: vasculogenesis that occurs in the developing embryo, and angiogenesis, which is the formation of new capillaries via sprouting or intussusception from pre-existing vessels [1].

Vasculogenesis occurs when the primary vascular plexus begins to form primitive blood vessels from angioblasts, which are the embryonic precursors of vascular endothelial cells [2]. After vasculogenesis occurs during embryonic development, new blood vessels are formed via angiogenesis. During the initiation of microvessel formation, there is a focal reduction both between interacting cells, as well as with the surrounding extracellular matrix (ECM), after which, deviation of pericytes occurs and endothelial cells begin to proliferate and migrate in either a sprouting manner or via intussusception. Finally, after the formation of endothelial cell networks via intussusception and cell sprouting, functional blood vessels are constructed by the processes of maturation and remodeling.

In contrast to embryonic vessel development, angiogenesis in adults is generally limited to wound healing and changes in female reproductive organs during the menstrual cycle and pregnancy. However, improper vascularization does occur in some pathological situations, such as ocular neovascularization, inflammatory diseases, and tumor formation [3]. Conversely, critical vascular regression can also cause defects in functional organs, such as myocardial infarction and the formation of pressure sores. Therefore, the development of techniques for the proper regulation of vascularization is of significant clinical interest [4,5].

Recently, regenerative medicine has become increasingly popular as a possible method for treating patients suffering from severe organ failure [6–8]. Ideally, via the combination of biotechnology and cell biology, functional tissues that resemble native structures can be created to replace damaged organs [9–11]. Yet, thus far a major obstacle has been the inability to maintain thick, viable tissues both

* Corresponding author. Fax: +81 3 3359 6046.
E-mail address: tokano@abmes.twmu.ac.jp (T. Okano).

0006-291X/$ - see front matter © 2006 Elsevier Inc. All rights reserved.
doi:10.1016/j.bbrc.2005.12.217

in vitro and in vivo, due to the lack of functional vascular network formation within the engineered constructs [12]. Therefore, it has become increasingly necessary to fabricate functional microvessels within engineered tissues, allowing for the proper supply of nutrients as well as, the removal of waste products, in order to avoid the core ischemia that is observed when tissue thickness is increased. However, while the steps involved in the normal development of blood vessels are well understood, the analogous mechanisms within engineered tissues remain unclear, and thus unable to be either controlled or manipulated. By clarifying these mechanisms of engineered tissue vascularization, approaches to create thicker tissues via the controlled development and manipulation of blood vessels may overcome one of the longstanding obstacles in tissue regeneration therapies.

Previously, we have demonstrated a novel method for tissue regeneration of cell sheet engineering, which uses temperature-responsive culture dishes [13]. With this technology, various types of cultured cells [14–18] can be non-invasively harvested as intact sheets via simple temperature reduction, without the need for proteolytic enzymes [19]. Therefore, vital cell-to-cell interactions that have been previously formed in culture can be maintained even during cell harvest [20]. When cardiac cell sheets were non-invasively harvested and layered in vitro, these three-dimensional constructs showed synchronous pulsations [21]. Upon subcutaneous transplantation of these bioengineered tissues, we also observed the in vivo formation of microvascular networks throughout the entire constructs, allowing for the long-term survival of the pulsatile tissues [21].

In the present study, we demonstrate the first step towards engineering vascularized tissues by elucidating the mechanisms of vessel reconstruction within these myocardial grafts created using cell sheet technology. Finally, after determining the processes involved in graft neovascularization, we show that by regulating endothelial cells within cell sheets, we can control the in vivo neovascularization.

Methods

All procedures using animals in this study were performed in accordance with the "Guide for the Care and Use of Laboratory Animals" (NIH Publication No. 85-23, revised 1996) published by National Institutes of Health, USA, and the "Guidelines of Tokyo Women's Medical University on Animal Use."

Temperature-responsive culture dishes. Specific procedures for the preparation of square-patterned temperature-responsive culture dishes (provided by CellSeed, Tokyo, Japan) have been previously described [22]. Briefly, *N*-isopropylacrylamide (IPAAm) monomer solution was spread onto commercial tissue culture polystyrene dishes. These dishes were then subjected to electron beam irradiation, resulting in polymerization and covalent bonding of IPAAm to the dish surface. Poly-IPAAm (PIPAAm)-grafted dishes were rinsed with cold distilled water to remove ungrafted IPAAm. Next, to prepare square-geometry PIPAAm-grafted cell culture dishes, the PIPAAm-grafted surfaces were masked with a square glass coverslip (24 × 24 mm, Matsunami, Osaka, Japan) and acrylamide (AAm) monomer (Wako Pure Chemicals, Tokyo, Japan) solution was spread onto the masked dish surface. The dish surface was then irradiated by electron beam and washed in the same manner. The resulting culture dishes thus had center square areas grafted with temperature-responsive PIPAAm with a surrounding border grafted with non-cell-adhesive poly-AAm. Culture dishes were finally sterilized by ethylene oxide gas.

Primary culture of neonatal rat cardiac cells. Ventricles from 1-day-old Wister rats (Nisseizai, Tokyo, Japan) were digested at 37 °C in Hanks' solution (Sigma, St. Louis, MO) containing collagenase (class II, Worthington Biochemical, Lakewood, NJ). Isolated cells were suspended in the culture medium comprising 6% FBS (Moregate Biotech, Bulimba, QLD, Australia), 35% Medium 199 (Invitrogen, Carisbad, CA, USA), 71.4 U/ml penicillin-solution, 71.4 μg/ml streptomycin-solution (Sigma, St. Louis, MO), 2.9 mM glucose, and 54% balanced salt solution containing 116 mM NaCl, 1.0 mM NaH_2PO_4, 0.8 mM $MgSO_4$, 1.2 mM KCl, 0.8 mM $CaCl_2$, and 26.2 mM $NaHCO_3$. Cell suspensions were plated at a density of 4.8×10^6 cells per square-geometry PIPAAm-grafted dish and incubated at 37 °C in a humidified atmosphere with 5% CO_2. For enhanced green fluorescent protein (EGFP)-positive cardiomyocytes, ventricles were isolated from EGFP-positive Sprague–Dawley (SD) neonatal rats [SD TgN (act-EGFP) OsbCZ-004], which were kindly provided by Prof. Masaru Okabe (Genome Information Research Center, Osaka University). For 2-methoxyestradiol (2-ME) or vascular endothelial growth factor (VEGF)-treated cells, after 1 day, the culture medium was replaced with fresh media containing either 2 μM 2-ME (Sigma, St. Louis, MO) or 10 nM VEGF (R&D Systems, Minneapolis, MN).

Immunocytochemistry. For endothelial cell staining, myocardial cell sheets were washed with Dulbecco's phosphate-buffered saline (PBS) and then fixed with 4% paraformaldehyde in PBS for 5 min at room temperature. Cells were washed again, blocked with 0.1% normal goat serum, and then incubated with a 1/200 dilution of anti-CD31 monoclonal antibody (Serotec, Oxford, UK) for 1 h at room temperature. A 1/200 dilution of anti-mouse IgG antibody conjugated with Alexa Fluor 488 (Invitrogen, Carlsbad, CA, USA) was applied for 1 h at room temperature as secondary antibody. Cell sheets were finally counterstained with Hoechst 33342 (Wako Pure Chemicals, Tokyo, Japan) for 5 min to visualize cell nuclei. Images were photographed by a AxioCam color digital camera (Carl Zeiss, Hallbergmoss, Germany) using fluorescence microscopy (ECLIPSE TE2000-U, Nikon, Tokyo, Japan) and processed with AxioVision 4.1 software. To quantify endothelial cell network formation, 1300 × 1030 pixel resolution images of cultured cell sheets were captured with a magnification of 40× or 100×. The area of CD31-positive cells in the sheets was calculated with NIH Image software. Data represent the average values of 20 or 5 images in each sample, respectively.

Gene expression analysis. mRNA expression of the angiogenesis-related genes, VEGF, cyclooxygenase (Cox)-2, tyrosine kinase with Ig and EGF homology domains (Tie)-2, Angiopoietin (Ang)-1, and Ang-2 within cardiomyocyte sheets was examined by RT-PCR analysis. Briefly, total RNA of the myocardial cell sheets cultured for either 3 or 7 days was isolated and purified using the RNeasy mini kit (Qiagen, Chatsworth, CA, USA). Reverse transcription was performed with the superscript II RT-PCR system (Invitrogen, Carlsbad, CA, USA) and subsequent PCR was performed with the MPCR Kit for Rat (Maxim Biotech, San Francisco, USA). PCR products were then electrophoresed on 4 % acrylamide gels and stained with ethidium bromide.

Manipulation of cell sheets into layered constructs. Neonatal rat myocardial cells were cultured for 4 days at 37 °C on square-designed temperature-responsive dishes. The culture dishes were set in another CO_2 incubator set at 20 °C to release confluent cells as contiguous cell sheets without enzyme treatments. Cardiomyocyte sheets detached spontaneously within 1 h and became slightly shrunken to about 1 cm^2 cell sheets due to cytoskeletal reorganization and sheet lateral traction forces. The entire cell sheet with media was gently aspirated into the tip of a pipette and the first sheet was transferred again onto a new temperature-responsive dish, with fresh media dropped onto the sheet to spread folded portions. After sheet spreading, media was aspirated and the dish was incubated at 37 °C to allow the cell sheet to fully adhere to the culture surface. To layer cell sheets, another cardiomyocyte sheet detached from a

PIPAAm-grafted dish was transferred and stacked onto the first cell sheet in the same fashion. An identical procedure was repeated to create triple-layer constructs in vitro.

Myocardial graft transplantation into dorsal subcutaneous tissues. EGFP-positive or negative male SD transgenic rats (4–5-weeks-old) or nude rats (4 weeks-old) were anesthetized with intraperitoneal injection of pentbarbital sodium (39 mg/kg). An L-shaped incision (approximately 3 cm × 2 cm) was made in the dorsal skin and lifting of the incised skin exposed the underlying tissue. Triple-layer cardiomyocyte sheets stacked on PIPAAm-grafted surfaces were detached again by lowering the culture temperature and washed with media. The cell constructs were lifted on top of a sterile polypropylene support sheet and transplanted onto dorsal subcutaneous tissues by sliding from the non-adhesive polypropylene sheet. The transplants were covered with 0.5-mm thick silicone membranes (Unique Medical, Tokyo, Japan) to prevent adhesion to the skin and the incisions were closed with 5-0 nylon sutures.

Histological analysis. At appropriate periods after transplantation, myocardial tissue grafts were excised and fixed in 10% neutral buffered formalin (Wako). Tissue specimens were then embedded in paraffin and sliced into 5 μm-thick sections. For hematoxylin and eosin staining, sections were processed by conventional methods. To detect GFP-expressing cells, cross-sections were immunolabeled with a 1/200 dilution of anti-GFP antibody (Invitrogen) for 16 h at 4 °C and secondary stained for 2 h with a 1/400 dilution FITC-conjugated anti-rabbit IgG antibody (Wako) for green fluorescence or Alexa Fluor 568-conjugated anti-rabbit IgG antibody (Invitrogen) for red fluorescence. To detect cardiomyocytes, cross-sections were immunolabeled with a 1/200 dilution of anti-α-sarcomeric actinin (Sigma) for 16 h at 4 °C and secondary stained for 2 h with Alexa Fluor 488-conjugated anti-mouse IgG antibody for green fluorescence or Alexa Fluor 568-conjugated anti-mouse IgG antibodies for red fluorescence. Vessel quantification was examined by counting the number of vessels per unit area, using hematoxylin and eosin stained sections.

Separation of endothelial cells from primary isolated cardiac cells. To regulate the ratio of endothelial cells in the myocardial cell sheets, endothelial cells were separated from primary myocardial cell suspensions by magnetic cell sorting (MACS). Briefly, primary myocardial cell suspensions were incubated with mouse monoclonal anti-rat CD31 antibody. After rinsing with running buffer (PBS containing 5% BSA and 2 mM EDTA), cells were incubated with anti-mouse IgG-conjugated microbeads (Miltenyi Biotec GmbH, Bergisch Gladbach, Germany) and then washed again with running buffer. The labeled cells were applied to the LS column in the magnetic fields of a MiniMACS system (Miltenyi Biotec GmbH, Bergisch Gladbach, Germany). The column was then washed with running buffer and removed from the magnetic fields, and cells trapped in the column were flushed out with running buffer. Endothelial cell-depleted cardiomyocyte suspensions were used to create cell sheets without endothelial cells. To fabricate myocardial cell sheets containing GFP-positive endothelial cells, GFP-negative cardiac cells (without endothelial cells), and purified GFP-positive endothelial cells were mixed in a ratio of 9:1.

Data analysis. All data are expressed as means ± SD. An unpaired Student's t test was performed to compare two groups. One-way ANOVA was used for multiple group comparison. If the F distribution was significant, a Tukey test was used to specify differences between groups. A p-value of less than 0.05 was considered significant.

Results

Angiogenic potential of cardiac cell sheets

To determine whether cardiac cell sheets possess innate potential for vessel formation, the presence of endothelial cells and the expression of angiogenesis-related genes of the cultured cell sheets were examined. Detection of the endothelial cell marker CD31 demonstrated that the pulsatile cardiac cell sheets contained significant amounts of endothelial cells and that the endothelial cells were arranged in a network-like formation after 4 days in culture (Fig. 1A). Gene expression analyses also showed that both VEGF and cyclooxygenase-2 (Cox-2), which are well-known angiogenesis-accelerating genes, were expressed continuously in the cultured cell sheets, in vitro (Fig. 1B). Significant mRNA expression of Tie-2, an endothelial cell-specific receptor, was also detected within the cardiac cell sheets (Fig. 1B). Correspondingly, Ang-1, a ligand of Tie-2, which is involved in the maturation process of blood vessel formation, was occasionally expressed, while Ang-2, which antagonizes Ang-1 binding to Tie-2, could not be detected (Fig. 1C). Taken together, these results indicate that the pulsatile cardiac cell sheets possessed their own potential for neovascularization, with the presence of endothelial cells in a network-like arrangement and the expression of major genes related to the promotion of vessel formation.

Endothelial cell network formation in cardiac cell sheets

To further examine the endothelial networks that were present within the cardiac cell sheets, the presence of CD31-positive cells was monitored throughout the culture period. One day after cell seeding, cardiomyocytes within the cell sheets began to pulsate asynchronously, but only a low number of sparsely distributed endothelial cells could be observed (Fig. 2A). At two days, the cells within the cardiac sheets began to beat synchronously and endothelial cells begin to proliferate and sprout within the sheets (Fig. 2B). Three days after initial cell seeding, the sprouting endothelial cells began to connect to each other (Fig. 2C) and at 4 days, these sprouting endothelial cells formed cell networks throughout the cardiomyocyte sheets (Fig. 2D). Quantification of the CD31-positive area within the cell sheets also showed that the area correlated to endothelial cells increased over time and accounted for 11.7 ± 5.9% of the total cell sheet area at 4 days (Fig. 2E). Additionally, these endothelial cell networks within the cardiac cell sheets were similar in appearance to the well-known sprouting form of endothelial cells cultured in Matri-gel. Finally, we also observed the occasional tubulogenesis of endothelial cells within the cardiac cell sheets, however these detected tubular structures had no continuity in vitro (data not shown).

To examine the reactivity of endothelial cells in cardiac cell sheets, cultured cells were treated with either 2-ME or VEGF, to examine their effects on network formation. In comparison to untreated controls, which showed an average of 8.0 ± 0.2% CD31-positive areas (Fig. 3A), after treatment with 2-ME, endothelial cell network formation was significantly diminished, representing only 0.3 ± 0.2% of the total area (Fig. 3B). In contrast, the addition of VEGF to the culture medium promoted endothelial cell network formation (13.6 ± 5.2%) (Fig. 3C), demonstrating that the cardiac cell sheets contained actively formed endothelial cell networks, having the characteristic nature of native blood vessels.